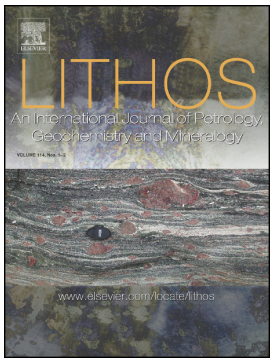

Dating agpaitic rocks: A multi-system (U/Pb, Sm/Nd, Rb/Sr and 40Ar/39Ar) isotopic study of layered nepheline syenites from the Ilímaussaq complex, Greenland

A.M. Borst, T.E. Waight, A.A. Finch, M. Storey, P.J.Le. Roux

PII: S0024-4937(18)30402-X
DOI: https://doi.org/10.1016/j.lithos.2018.10.037
Reference: LITHOS 4853

To appear in: *LITHOS*

Received date: 13 June 2018
Accepted date: 31 October 2018

Please cite this article as: A.M. Borst, T.E. Waight, A.A. Finch, M. Storey, P.J.Le. Roux , Dating agpaitic rocks: A multi-system (U/Pb, Sm/Nd, Rb/Sr and 40Ar/39Ar) isotopic study of layered nepheline syenites from the Ilímaussaq complex, Greenland. Lithos (2018), https://doi.org/10.1016/j.lithos.2018.10.037

Dating agpaitic rocks: A multi-system (U/Pb, Sm/Nd, Rb/Sr and $^{40}Ar/^{39}Ar$) isotopic study of layered nepheline syenites from the Ilímaussaq complex, Greenland

A.M. Borst[1,2,3,*] amb43@st-andrews.ac.uk, T.E. Waight[2], A. A. Finch[3], M. Storey[4], P. J. Le. Roux[5]

[1]Department of Petrology and Economic Geology, Geological Survey of Denmark and Greenland, Øster Voldgade 10, 1350 Copenhagen, Denmark

[2]Department of Geosciences and Natural Resource Management (Geology Section), University of Copenhagen, Øster Voldgade 10, 1350, Copenhagen, Denmark

[3]School of Earth and Environmental Sciences, University of St Andrews, Irvine Building, North Street, St Andrews, United Kingdom

[4]Quadlab, Natural History Museum of Denmark, Øster Voldgade 5-7, 1350, Copenhagen, Denmark

[5]Department of Geological Sciences, University of Cape Town, Rondebosch 7701, South Africa

[*]Corresponding author at: School of Earth and Environmental Sciences, University of St Andrews, North Street, St Andrews, Fife KY16 9AL, United Kingdom.

ABSTRACT

The Ilímaussaq complex in southern Greenland is a shallow crustal composite intrusion comprising augite syenite, peralkaline granite and volumetrically dominant agpaitic nepheline syenites. Previous studies indicated a zircon U-Pb age of 1160 ± 5 Ma for the augite syenite, the earliest intrusive unit of the complex. A similar crystallization age, within error, is inferred for the main sequence of agpaitic nepheline syenites. However, direct age determination of these units has been challenging because agpaitic rocks characteristically lack robust phases for *in situ* U-Pb dating (e.g. zircon/baddeleyite). An additional challenge is the pervasive subsolidus alteration, of which the isotopic effects are poorly constrained. Here we present new U-Pb, Sm-Nd and Rb-Sr isotopic data from whole rocks and mineral separates and a $^{40}Ar/^{39}Ar$ amphibole age of three co-genetic agpaitic nepheline syenites (kakortokite) from the lowermost exposed part of the complex. Using a multi-system geochronological approach for mineral separates and whole rocks, we explore the effects of late-stage alteration for each isotopic system. Assuming a closed-system evolution for the hydrothermal fluids (i.e. isotopically similar to the melts) and cooling within a relatively short time-frame (<0.8 Ma), we evaluate whether traditional mineral-whole rock isochron methods can provide useful age constraints for agpaitic rocks. We compare our data with those in the literature, corrected for the most recent decay constants.

Single-crystal $^{40}Ar/^{39}Ar$ step-heating experiments yield an amphibole plateau age of 1156.6 ± 1.4 Ma (MSWD=1.5, external error ± 7.7 Ma), which we put forward as the most precise crystallization age for the agpaitic units to date. Kakortokite whole rock and mineral separates (amphibole, eudialyte, feldspar) yield a ^{206}Pb-^{207}Pb isochron age of 1159 ± 17 Ma (MSWD=0.96) and a ^{235}U-^{207}Pb isochron age of 1168.5 ± 8.8 Ma (MSWD=0.82). These are within error of the zircon and baddeleyite U-Pb ages from the augite syenite, as well as the

new plateau age, if we take into account the external error of 7.7 Ma (i.e. accuracy). The ^{235}U-^{207}Pb age thus far provides the best non-single mineral age estimate for the agpaitic suite. Sm-Nd isotopes for the same whole rock and mineral separates yield an isochron age of 1156 ± 53 Ma (MSWD=0.23) with ε_{Ndi} = -0.8 ± 0.8, with significantly less scatter than Nd data for the rest of the complex. Rb-Sr isotopes yield errorchron ages that are either unrealistically young (3-point feldspar errorchron: 1106 ± 9 Ma, suggesting partial ^{87}Sr loss), or old (WR, amphibole and eudialyte: 1237 ± 21 Ma, n=9). The data demonstrate that the U-Pb and Sm-Nd systems are relatively insensitive to late-magmatic alteration and re-equilibration during cooling. In contrast, the Rb-Sr system records significant disturbance, reflecting the highly mobile nature of Rb and Sr in peralkaline systems. This warrants careful reconsideration of previously published Rb-Sr isochron data, and caution in interpreting Rb-Sr data for other peralkaline complexes. Initial isotopic compositions for the kakortokite support petrogenetic models that describe Ilímaussaq melt evolution towards strongly radiogenic Sr values at relatively constant $\varepsilon_{Ndi,}$ with progressive evolution from the early augite syenite to the most fractionated agpaitic melts. The melts experienced variable but minor degrees of lower crustal assimilation and/or preferential leaching of radiogenic Sr from the Proterozoic granitic country-rock.

Keywords: Geochronology; Agpaitic nepheline syenites; Peralkaline rocks; Ilímaussaq; Radiogenic isotopes; Eudialyte

INTRODUCTION

Agpaitic nepheline syenites crystallize from highly peralkaline and halogen rich melts, and are associated with economically important deposits of High Field Strength Elements (HFSE) including Zr, Nb, Ti and Hf and the Rare Earth Elements (REE). Petrographically, agpaitic nepheline syenites are identified by the presence of complex Na-Ca-HFSE-silicates such as eudialyte- and rinkite-group minerals, instead of more common (miaskitic) HFSE-phases such as zircon, baddeleyite and titanite (e.g. Ussing, 1912; Sørensen, 1997; Marks *et al.*, 2011). Since U-Pb age determination of zircon and baddeleyite are one of the main tools of geochronology, obtaining precise and accurate age constraints from agpaitic rocks in which these minerals are absent is a challenge. Furthermore, due to their volatile-rich nature, agpaitic rocks typically experience intense autometasomatic alteration by late-stage hydrothermal fluids (e.g. Kogarko, 1974; Marks and Markl, 2017; Mitchell and Liferovich, 2006; Borst *et al.*, 2016). These processes lead to complex magmatic-hydrothermal replacement reactions and can remobilize elements and disturb isotopic systems. Alternative routes need to be determined for the precise and accurate geochronology of agpaitic rocks. Crystallization ages for agpaitic rocks have mostly been derived from Rb-Sr isochrons (e.g. Blaxland *et al*, 1976b; 1978; Finch *et al.*, 2001; Kramm & Kogarko, 1994; Waight *et al.*, 2002), or $^{40}Ar/^{39}Ar$ dating (Krumrei *et al.*, 2006). Alternatively, agpaitic suites have been dated indirectly by U-Pb dating of suitable phases from contemporaneous non-agpaitic rocks, late-stage hydrothermal assemblages or associated fenitized country rocks (e.g. Krumrei *et al.*, 2006; Estrade *et al.*, 2014; Möller and Williams-Jones, 2016; Sjöqvist *et al.*, 2017).

The present study is a detailed petrological and isotopic study of a co-genetic, modally-layered unit within macro-rhythmically layered agpaitic nepheline syenites (kakortokite) of the Ilímaussaq complex in South Greenland. Ilímaussaq represents a shallow intrusive complex that was emplaced in the final stages of the Mesoproterozoic Gardar rifting event

(Upton *et al.*, 2013). We present new Ar-Ar, Rb-Sr, Sm-Nd and U-Pb isotopic data for mineral separates and whole rocks from the kakortokite and contrast the precision and accuracy of each method. We compare our data critically with published isotope studies of other agpaitic units in the complex. Given the pervasive hydrothermal alteration associated with agpaitic rocks, we explore the susceptibility of each isotope system to post-magmatic modification, thereby providing insights not only into the most accurate methods of geochronology, but also the isotopic expression of the alteration. Finally, we draw conclusions about the best routes to the accurate and precise geochronology of agpaitic rocks.

GEOLOGICAL SETTING

The Ilímaussaq complex belongs to the Mesoproterozoic Gardar Province in South Greenland; a two-stage continental rift zone associated with the breakup of the Columbia supercontinent (rifting between 1300-1250 Ma and 1180-1140 Ma; Upton (2013) and references therein). The province hosts over a dozen plutonic complexes and dyke swarms, spanning a compositional range from alkali basalt to trachyte, through to alkali granite and strongly peralkaline nepheline syenite, as well as carbonatite and lamprophyre (e.g. Upton and Emeleus, 1987; Upton *et al.*, 2003; Upton, 2013; Bartels *et al.* 2015). Importantly, no regional metamorphism occurred in the Gardar region following rifting (Upton and Emeleus, 1987; Upton *et al.*, 2003; Upton, 2013; Marks and Markl, 2015) and so most Gardar rocks remain undisturbed since emplacement. The Ilímaussaq complex is part of the younger Gardar rift and comprises some of the most evolved and volatile-rich peralkaline magmas in the province. The complex was emplaced at c. 3-4 km depth (fluid inclusion data, Konnerup-Madsen and Rose-Hansen, 1984) at the contact between granitic Ketilidian basement (1.7-1.8 Ga) and interbedded basalts and sandstones of the early Gardar Eriksfjord Formation (Upton,

2013 and references therein). Emplacement and cooling of the complex is inferred to have occurred within 0.5-0.8 Ma (Krumrei *et al.,* 2006).

The complex is renowned for its spectacular magmatic layering, mineralogical diversity and multi-element resource potential in rare earth elements (REE), Zr, Nb, U, Li, Be and Zn (Bailey *et al.,* 2001; Larsen and Sørensen, 1987; Sørensen, 1992). The rocks crystallized from at least four melt batches derived from a common, deep-seated magma chamber (e.g. Sørensen *et al.,* 2006). The first batch crystallized as metaluminous augite syenite, exposed in the roof and as a marginal rim around the complex (Fig 1). The second batch formed a thin sheet of peralkaline granite and quartz syenite, found only in the roof of the complex. This was followed by medium to strongly Si-undersaturated peralkaline nepheline syenite melts (e.g. Ferguson, 1964; Larsen and Sørensen, 1987; Sørensen *et al.,* 2006; Marks and Markl, 2015). The latter are structurally divided into (i) a downward crystallized sodalite-rich 'roof' series (mostly naujaite), (ii) an upward crystallized, rhythmically layered 'floor' series (kakortokite) and (iii) an intervening sandwich horizon of the most evolved melts (lujavrites) (Fig. 1). With the exception of the earliest roof units, all rocks are agpaitic and thus contain sodic minerals such as elpidite ($Na_2ZrSi_6O_{15}.3H_2O$), eudialyte ($Na_{15}Ca_6Fe_3Zr_3Si_{26}O_{72}(O,OH,H_2O)_3(Cl,OH)_2$) and rinkite ($Na_2Ca_4REE(Ti,Nb)(Si_2O_7)_2(O,F)_4$) as dominant carriers of HFSE. The agpaitic nepheline syenite units from this last batch of magma are mineralogically similar, but differ in texture and modal proportions of the major minerals: nepheline, eudialyte, sodalite, alkali feldspar, Na-Fe-amphibole (arfvedsonite) and Na-Fe-pyroxene (aegirine). Although the roof, middle and floor series were originally interpreted as differentiation products of a single melt (Ussing, 1912; Ferguson, 1964; Larsen and Sørensen, 1987; Sørensen, 1997), the roof series (naujaite) and the kakortokite-lujavrite series are now interpreted to have crystallized from at least two separate melt batches (Sørensen *et al.,* 2006; Ratschbacher *et al.,* 2015).

Here we focus on the lowermost exposed rocks in the complex, known by the local term 'kakortokite'. These medium-coarse grained agpaitic nepheline syenites form a c. 220 m thick rhythmic sequence of at least 29 tripartite modally-layered units. Each unit is ~8 m thick, comprising a basal black layer enriched in arfvedsonite (c. 1 m), grading into a thin eudialyte-rich layer (c 0.5 m, sometimes difficult to observe), followed by a thick upper white layer (c. 7 m) enriched in alkali feldspar and nepheline (Fig. 2) (Bohse *et al.*, 1971; Bohse and Andersen, 1981, Hunt *et al.*, 2017). The precise origin of the rhythmic modal layering remains controversial. Proposed models range from density separation, mat formation and mush processes within a rising crystallization front (Bons *et al*, 2016; Lindhuber *et al.*, 2015, Borst *et al.*, 2018) to nucleation cycles induced by periodic volatile release or repeated melt influx (Pfaff *et al.*, 2008; Hunt *et al.*, 2017). All models, however, agree that each individual black-red-white kakortokite unit crystallized from a homogeneous melt representing a chemically closed-system.

An important aspect of agpaitic rocks is that they crystallize from unusually volatile-rich (F, Cl, OH) and reduced melts over extended temperature intervals (c. 1000-450˚C, e.g. Markl *et al.*, 2001; Marks and Markl, 2017). Low oxygen fugacity is thought to play an important role in that it suppresses the exsolution of aqueous fluid phases at the early magmatic stage, leading to the extreme enrichment in alkalis and HFSE as the melt evolves (e.g. Markl *et al.*, 2001; 2010). Consequently, agpaitic melts straddle evolution from discrete silicate melt to silica-bearing aqueous fluids (Kogarko, 1974). This results in pervasive late-stage hydrothermal vein and pegmatite formation, and autometasomatic replacement of primary phases by low-temperature secondary mineral assemblages (e.g. Marks and Markl, 2015; 2017; Markl and Baumgartner, 2002; Mitchell and Liferovich, 2006). In the kakortokite at Ilímaussaq, this is expressed in the widespread replacement of cumulus eudialyte by secondary Zr, Nb and REE-silicates, zeolitic replacement of primary

aluminosilicates and replacement of arfvedsonite by secondary aegirine and Fe-oxides (e.g. Karup-Møller *et al.*, 2010; Borst *et al.*, 2016; Marks & Markl, 2015). Despite the importance of the hydrothermal alteration, and the large volume of isotopic data, the isotopic effects of late-stage alteration have not previously been studied.

PREVIOUS GEOCHRONOLOGICAL STUDIES

There have been many attempts to date the Ilímaussaq complex (Table 1). Ages reported in the literature include *in situ* zircon and baddeleyite U-Pb ages of 1166 ± 9 Ma (unpublished from Heaman and Upton, cited in Upton *et al.*, 2003) and 1160 ± 5 Ma (Krumrei *et al.*, 2006), respectively, from the first intrusive unit (the augite syenite). Published radiogenic isotopic data for the main agpaitic suite include a whole rock Rb-Sr isochron age of 1162 ± 21 Ma[1] (Blaxland *et al.*, 1976b), a two-mineral Rb-Sr age of 1179 ± 2.3 Ma (Waight *et al.*, 2002) and three polylithionite (Li-K-mica) Rb-Sr ages with an average of 1081 ± 24 Ma (Moorbath *et al.*, 1960). Sm-Nd isotopic studies have yielded poorly constrained, but statistically identical whole rock-mineral isochron ages of 1130 ± 50 Ma (augite syenite, Paslick *et al.*, 1993), 1160 ± 30 Ma (all units, Marks *et al.*, 2004), as well as an *in situ* eudialyte isochron age of 1128 ± 63 Ma (by laser ablation ICPMS; Wu *et al.*, 2010). $^{40}Ar/^{39}Ar$ amphibole ages (Krumrei *et al.*, 2006) range between 1142.6 ± 2.2 to 1152.3 ± 3.7 Ma, calculated using the ^{40}K decay constant after Steiger and Jäger (1977). However, the statistical validity of the plateau ages was questioned by Baksi (2007) and the $^{40}Ar/^{39}Ar$ ages require re-evaluation in light of recent advances in the precision and accuracy of the ^{40}K

[1] Rb-Sr ages are recalculated using a Rb decay constant of 1.397 x 10^{-11} a^{-1} (Villa *et al.*, 2015a). Note that the age of Waight *et al.* (2002) becomes older than reported, whereas the others become younger. This is due to different decay constants used in the original studies (1.42 and 1.39 x 10^{-11} a^{-1}, after Steiger and Jager (1977) and Aldrich *et al.* (1956), respectively).

decay constant and Fish Canyon Tuff (FCT) monitor age (Kuiper *et al.*, 2008; Rivera *et al.*, 2011; Renne *et al.*, 2010, 2011).

SAMPLES AND PETROGRAPHY

Samples for isotopic study were collected from a single co-genetic kakortokite unit, known as Unit 0. Unit 0 is distinguished by its striking, arfvedsonite-rich basal layer (*c.* 0.8 m), sharp lower contact and an anomalously thick (*c.* 2 m) eudialyte-rich middle red layer (Fig. 2). The unit is used as a marker horizon relative to which the other units are numbered (-11 to +17; Bohse *et al.*, 1971). Representative samples of the black, red and white layers from unit 0 were taken along a vertical section of *c.* 3 m in the Laksetværelv valley (coordinates 60.881092 N, -45.829266 W; *c.* 70 m altitude, Fig. 1) and crushed for whole rock powder and mineral separation. In total, three whole rocks (a black, red and white kakortokite) and nine mineral separates (eudialyte, arfvedsonite amphibole, perthitic alkali feldspar) were prepared. For the purpose of this study, we meticulously picked fresh samples that display minimum evidence for alteration. Detailed petrographic, textural and compositional data for unit 0 are available in e.g. Bohse *et al.* (1971), Bohse and Andersen (1981), Pfaff *et al.* (2008), Marks and Markl (2015), Lindhuber *et al.* (2015), Hunt *et al.* (2017) and Borst *et al.* (2018). The samples studied are briefly described below and are all in the collections of the Geological Survey of Denmark and Greenland.

Black kakortokite

The black kakortokite (535019-0B, Fig. 2d) contains 50-60% modal arfvedsonite and c. 10% primary aegirine, both occurring as euhedral cumulus and interstitial grains (c. 1-3 mm).

Some arfvedsonite contains small (<0.2 mm) inclusions of fluorite and apatite (Fig. 3c). Feldspar occurs as tabular, coarsely-exsolved perthite, measuring *c.* 0.5 to 1.5 mm in width and up to 5 mm in length and generally consisting of K-feldspar rich cores with irregular patches and rims of turbid albite. They make up *c.* 25-35% of the mode and define a magmatic lamination parallel to the unit boundaries, along with amphibole (Fig. 2d). Nepheline (10-15%) forms patchy equant grains (0.5-1 mm) trapped between feldspar laths and cumulus amphibole. They contain inclusions of arfvedsonite, aegirine needles and other phases, and are locally replaced by zeolites (mostly analcime and natrolite, Fig. 3d). Eudialyte is a minor component (5-10%) in the black kakortokite, and forms euhedral crystals of *c.* 0.5-2 mm. The eudialyte is locally replaced by catapleiite (hydrous Na-Zr-silicate), aegirine, analcime, nacareniobsite-(Ce) and other REE- and Nb-phases (Borst *et al.*, 2016; Fig. 3a). Sodalite and fluorite are minor interstitial phases.

Red kakortokite

The red kakortokite (535020-0R, Fig. 2c) has a saccharoidal texture with *c.* 40% euhedral eudialyte, 15-20% sub- to euhedral nepheline and a few dispersed larger (>5 mm) subhedral sodalite grains (*c.* 5%). Alkali feldspar laths in the red kakortokite are stubbier (*c.* 1 by 3 mm) than in the black and white kakortokite and make up approximately 15-20% of the mode. Arfvedsonite (10-15%) and aegirine (*c.* 5%) are interstitial phases and often poikilitically overgrow eudialyte, nepheline and occasionally sodalite (Fig. 3a). Fluorite and rinkite both form accessory phases, with rinkite occurring either interstitially or in clusters of euhedral long-prismatic crystals.

White kakortokite

The white kakortokite (535021-0W, Fig. 2b) is coarser-grained and exhibits a laminated texture with an interlocking framework of elongated (up to 6 mm) feldspar laths (35-45%), sub- to eu-hedral nepheline (20-30%), euhedral eudialyte (5-15%) and sodalite (5-10%). As in the red kakortokite, arfvedsonite and aegirine typically occur interstitially. Fluorite and rinkite are slightly more abundant (<5%) than in the black and red layer. Arfvedsonite is partially replaced by secondary aegirine (aeg-II) and locally contains small subrounded (>20 μm) inclusions of fluorite and fluorapatite (Fig. 3b,c). As in the other samples, some eudialyte grains are partially to completely replaced by aggregates of secondary catapleiite, aegirine, nacareniobsite and other minerals (Fig. 3d; Borst *et al.*, 2016). Feldspars and feldspathoids are partially replaced by zeolites along their margins.

Analytical Methods

A full description of analytical procedures is present in the Supplementary Information but a brief description is given here. Fresh mineral separates of eudialyte, alkali feldspar and amphibole were meticulously handpicked from a 250-500 μm size fraction using an optical microscope. Only optically clear grains were chosen to avoid alteration and impurities. Altered eudialyte could readily be distinguished from pink, glassy eudialyte, because of the murky beige to brown colours of the alteration products (Borst *et al.*, 2016). Arfvedsonite grains partially replaced by secondary aegirine could be readily identified by a distinct brownish colour and the dull lustre of the aegirine. Distinguishing primary arfvedsonite (lustrous black green) from primary aegirine (brighter dark green) was more difficult, and so some primary aegirine may be present in the separates. For the feldspar separates, only euhedral laths were picked to avoid analcime, natrolite and other secondary (low-temperature) aluminosilicates. Despite careful picking the presence of some alteration

products or inclusions (e.g. fluorite, fluorapatite, aegirine) in the mineral separates cannot fully be discounted.

Rb-Sr, Sm-Nd and Pb (isotope dilution) measurements were carried out by TIMS at the University of Copenhagen, Denmark, using methods similar to Scott *et al.* (2014). U, Pb (isotopic composition) and Nd on selected low-Nd samples and two eudialyte duplicates were analyzed by MC-ICPMS at the University of Cape Town, South Africa. Rb-Sr, Sm-Nd and U-Pb isochron regressions were calculated with Isoplot Version 4.15 (Ludwig, 2003), using blanket errors based on the external reproducibility of standards (Supplementary data). Decay constants used are listed in Table 1. Initial ratios and ε_{Ndi} values are calculated using present day CHUR $^{147}Sm/^{144}Nd$ ratios of 0.1967 (Jacobsen and Wasserburg, 1980) and $^{143}Nd/^{144}Nd$ of 0.512638 (Goldstein *et al.*, 1984), and an Ilímaussaq emplacement age of 1160 Ma. The uncertainty of reproducibility on the calculated ε_{Ndi} values corresponds to ±0.3 ε-units. Depleted mantle model ages (T_{DM}) are calculated using present day $^{147}Sm/^{144}Nd$ and $^{143}Nd/^{144}Nd$ values of 0.219 and of 0.513151 (Liew and Hofmann, 1988).

Handpicked amphibole grains were selected for single crystal step-heating $^{40}Ar/^{39}Ar$ experiments using a Nu Instruments Noblesse multi-collector noble gas mass spectrometer at the Quaternary Dating Laboratory (QUADLAB), Natural History Museum of Denmark. Grains were cleaned in ethanol and distilled water, then wrapped in aluminium foil and irradiated for 60 hours at the Cd-lined CLICIT facility at the Oregon State University TRIGA Reactor (USA), along with FCT sanidines (28.172 Ma; Rivera *et al.*, 2011) as the neutron-flux monitor for J calculation. Step-wise heating was achieved using a defocused CO_2 laser beam by incrementally increasing its power. The analytical procedures, decay constants and isotopic compositions used are as described in Rivera *et al.* (2011), and summarized in the Supplementary Data. Plateau ages are calculated at the 95% confidence level, and require at least three contiguous gas fractions with ages indistinguishable within analytical error (± 2σ)

which together account for a significant fraction of the total gas released (ideally >50%, Baksi, 2007 and references therein). For grains that do not yield plateau ages by those criteria, an age approximation is given as the integrated total gas age calculated by weighting each step age against the fraction of ^{39}Ar released.

RESULTS

5.1 U-PB DATA

Pb isotopic data are given in Table S1 (Supplementary Data) and shown in Figure 4. The kakortokite minerals and whole rocks define a $^{207}Pb/^{206}Pb$ isochron that yields an age of 1159 ± 17 Ma (MSWD=0.96, Fig. 4a). The most radiogenic sample is the alkali feldspar from the red kakortokite (535019-fsp) with a $^{206}Pb/^{204}Pb$ ratio of 33, followed by feldspar, amphibole and eudialyte of the white kakortokite. Other samples, including the white kakortokite whole rock, cluster between $^{206}Pb/^{204}Pb$ ratios of 18-20. In the conventional U-Pb isochron diagrams (Fig. 4b, c) three points deviate from the general trend (535020-arf, 535021-fsp and 535021-arf). A regression that excludes these 'outliers' yields a ^{238}U-^{206}Pb errorchron of 1173 ± 16 Ma (MSWD=11.3, Fig 4b) and a ^{235}U-^{207}Pb isochron of 1168.5 ± 8.8 Ma (MSWD =0.82, Fig. 4c), i.e. both within error of the published augite syenite and alkali granite U-Pb ages and our kakortokite $^{207}Pb/^{206}Pb$ isochron (Table 1). Initial ratios are $^{206}Pb/^{204}Pb$ = 16.02 ± 0.09 and $^{207}Pb/^{204}Pb$ = 15.234 ± 0.007.

5.2 SM-ND DATA

Sm-Nd concentrations and isotope compositions are given in Table S2 and shown in Figure 5. Alkali feldspar has the lowest REE concentrations (1-2 ppm Sm and 3-13 ppm Nd), and arfvedsonite only slightly higher (4-7 ppm Sm and 36-44 ppm Nd). Eudialyte is the main REE-bearing phase with 614 - 645 ppm Sm and 3055 - 3273 ppm Nd. Rare earth contents are relatively constant in the three eudialyte separates. Whole rock concentrations strongly reflect

respective mineral proportions, with the highest Sm and Nd contents in the red kakortokite (363 ppm Sm and 1829 ppm Nd) and lower concentrations in black and white (70-74 ppm Sm and 368-394 ppm Nd). The samples exhibit a relatively narrow range in Sm/Nd ratios from 0.13 in arfvedsonite to 0.2 in eudialyte, consistent with the light rare earth enriched patterns characteristic for most Ilímaussaq rocks and minerals (e.g. Bailey *et al.*, 2001; Pfaff *et al.*, 2008). An age regression for the TIMS and MC-ICPMS data that excludes three outliers (535021-arf, 535019-fsp, and 535020-wr) gives an age of 1156 ± 53 Ma (MSWD = 0.23, n = 11) with an intercept at $^{143}Nd/^{144}Nd_i$ = 0.51110 ± 4, corresponding to ε_{Ndi} = -0.8 ± 0.8 (Fig. 5).

5.3 Rb-Sr data

Rb-Sr concentrations and isotope compositions are presented in Table S3 and Fig. 6. As also demonstrated by Waight *et al.* (2002), the alkali feldspars are characterized by extremely high Rb/Sr ratios (80-157) and associated radiogenic $^{87}Sr/^{86}Sr$ ratios (6-23.4). Eudialyte is the main host for Sr (*c.* 450-600 ppm), as mirrored in the relatively high Sr whole rock concentrations for red kakortokite (Fig. 5; XRF data from Bailey *et al.*, 2001). In contrast, Rb is relatively incompatible in eudialyte, yielding low $^{87}Rb/^{86}Sr$ ratios (<0.14) and $^{87}Sr/^{86}Sr$ close to initial values. Amphiboles have Rb/Sr ratios close to 2 ($^{87}Rb/^{86}Sr$ ratios *c.* 6). Whole rock Rb/Sr ratios vary between 0.9 and 6.6 and strongly reflect the respective modal abundances of arfvedsonite, eudialyte and alkali feldspar. A best-fit regression through all samples yields an errorchron age of 1091 ± 6.3 Ma with extreme scatter (MSWD = 10737) and a poorly constrained $^{87}Sr/^{86}Sr_i$ = 0.702 ± 0.046 (Fig. 6a).

The feldspar data alone define a three-point errorchron of 1106 ± 94 Ma with a MSWD of 25 and a poorly constrained $^{87}Sr/^{86}Sr_i$ of 0.5 ± 1.4. Excluding feldspar, the whole rock, arfvedsonite and eudialyte give a steeper slope: a regression excluding feldspar and outlier

535021-arf yields a geologically meaningless age of 1237 ± 21 Ma (MSWD = 9811) with $^{87}Sr/^{86}Sr_i = 0.707 \pm 0.003$.

5.4 ^{40}Ar-^{39}Ar DATA

Amphibole grains from the black kakortokite (535019) were dated by single crystal $^{40}Ar/^{39}Ar$ step-heating in 4 separate experiments (Supplementary Data Table 4). Gas release spectra are shown in Figure 7. Two out of four grains display release patterns that meet the criteria for calculating $^{40}Ar/^{39}Ar$ plateau ages. One of these forms a well-defined plateau (535019-arf3) giving an age of 1156.6 ± 1.4 Ma (internal error) with MSWD = 1.5 and p = 0.20 (Fig. 7b), including 5 steps and accounting for more than 99% of the total ^{39}Ar released. The second plateau (535019-arf4) yields an age of 1155 ± 2 Ma (MSWD=2.34, p = 0.10) for 3 steps and 45.7% of the total gas released (Fig. 7c). Although the MSDW is too high (>2) and the total gas released too low (< 50%) to be considered a robust plateau age, the age is within uncertainty of the plateau age for 535019-arf3. The two remaining grains (Fig. 7a, d) do not meet the criteria for a plateau age and their ages are approximated by total gas ages of 1149 ± 0.9 Ma and 1155 ± 2 Ma, respectively. All grains released minor argon (<0.8% of $^{39}Ar_{tot}$) in the first heating step with isotopic compositions yielding young ages of c. 600-770 Ma, associated with lower % $^{40}Ar^*$ (<85%), and larger Ca/K and analytical errors. In subsequent heating steps, all grains degas relatively continuously, with the bulk of their total ^{39}Ar (>75%) released in the 2-3 W laser power interval (steps 2-5). Most of the gas-rich steps have isotopic compositions associated with step ages in the range of 1151 ± 0.7 to 1163 ± 4.5, with some outliers mainly towards younger ages (Supplementary data). All grains reveal an increase in Ca/K ratios in the last gas fractions released, notably in the step prior to fusion (Fig. 7). This is reflected by a factor of 5 increase in the $^{37}Ar/^{39}Ar$ ratios, due to ^{37}Ar produced from ^{40}Ca.

DISCUSSION

Data obtained in the current study permit a direct comparison of U-Pb, Sm-Nd and Rb-Sr isochron ages with single crystal ^{40}Ar-^{39}Ar ages from a single co-magmatic agpaitic unit. The data allow us to evaluate the sensitivity of each mineral and isotope system to late-stage equilibration and hydrothermal alteration. Below we compare the kakortokite isochron data to reported ages from other intrusive units of the Ilímaussaq complex, and re-evaluate those ages in light of modern decay constants. Isotopic systems are discussed individually before a final evaluation of geochronological techniques is made. Additionally, the petrogenetic significance of more precisely determined initial isotopic compositions for the kakortokite melts are discussed.

6.1 U-PB SYSTEMATICS

The kakortokite samples form a well-defined $^{207}Pb/^{204}Pb$-$^{206}Pb/^{204}Pb$ isochron age that matches the baddeleyite and zircon U-Pb ages of Krumrei *et al.* (2006) and Upton and Heaman, cited in Upton (2003) (Fig. 4a). Isochron plots for the individual U-Pb decay systems reveal three outliers, i.e. two arfvedsonite samples and one feldspar. The fact that only their U/Pb ratios, and not the $^{207}Pb/^{204}Pb$ and $^{206}Pb/^{204}Pb$ ratios, are affected may point to potential issues with the chemistry or the analytical procedure for U. For example, issues with spiking, weighing or contamination, differences in mass fractionation between sample and standard or interference corrections due to insufficient chemical purification of U. However, if the anomalous U/Pb data are indeed a consequence of geological disturbance of U and/or Pb, this must be due to a relatively recent event. Recent loss or gain of U or Pb loss could explain the offsets in the $^{238}U/^{204}Pb$ and $^{235}U/^{204}Pb$ ratios and would not affect the radiogenic Pb ratios, as observed here (Fig. 4). Isotopic disturbance immediately after crystallization would not be visible in either U/Pb or $^{207}Pb/^{204}Pb$-$^{206}Pb/^{204}Pb$ isochrons, whereas partial or

complete resetting at a given time after crystallization would result in offsets in both diagrams. The latter scenarios can be excluded, and the preferred explanation is recent disturbance of U and/or Pb loss. It is noteworthy that the whole rocks from which the three outlier minerals were separated fall on the isochron trend, suggesting isotopic equilibrium was maintained on a whole rock scale.

Published U-Pb work on the agpaitic suite is limited to *in situ* U-Pb analyses of eudialyte by Wu *et al.* (2010), which gave relatively young $^{206}Pb/^{238}U$ ages between 1018 ± 34 and 1134 ± 29 Ma (Table 1; Fig. 11) considered to reflect Pb loss after crystallization. Calculation of $^{207}Pb/^{206}Pb$ ages, e.g. not affected by Pb loss, was not possible from *in situ* analyses because of the necessity to correct ^{207}Pb for high common Pb in eudialyte. Attempts to retrieve age information from secondary zircon in the 'hybrid' part of the kakortokites, i.e. genetically related agpaitic nepheline syenites, were also unsuccessful due to very low U contents and high common Pb (Hunt, Pers. Comm., 2017). The whole rock-mineral isochron method by isotope dilution does not require a common Pb correction, and so is more suitable for U/Pb dating of agpaitic rocks. Both the ^{207}Pb-^{206}Pb isochron age (1159 ± 17 Ma) and individual U-Pb isochron ages (1173 ± 16 and 1168.5 ± 8.8 Ma) are consistent with the baddeleyite and zircon U-Pb ages (Fig. 4, Table 1) and are thus considered accurate independent ages for the kakortokite, although somewhat less precise.

6.2 Sm-Nd systematics

Figure 8 compares our data to published Sm-Nd data for Ilímaussaq lithologies from Paslick *et al.* (1993), Stevenson *et al.* (1997) and Marks *et al.* (2004) and illustrates the narrow range of Sm/Nd ratios in all Ilímaussaq rocks and minerals ($^{147}Sm/^{144}Nd$ between 0.05-0.15). The published Nd data show a considerable range in initial $^{143}Nd/^{144}Nd$, corresponding to ε_{Ndi} between +0.4 and -5.7. The augite syenite records the most radiogenic Nd values, while the majority of agpaitic samples plot within uncertainty of our calculated regression (shaded area,

Fig. 8). Samples with low Nd isotopic values, plotting below the 1160 Ma trend, have been interpreted by Marks *et al.* (2004) and Stevenson *et al.* (1997) to reflect minor degrees of lower crustal assimilation and local wall-rock contamination (see discussion below).

Our kakortokite Sm-Nd data show significantly less scatter relative to earlier datasets (Fig. 8), which we interpret to reflect their derivation from a single co-genetic kakortokite unit. Our kakortokite regression, using blanket errors based on the external reproducibility of standards, yields an age of 1156 ± 53 Ma (MSWD = 0.23, n= 11) with an initial $^{143}Nd/^{144}Nd$ of 0.51110 ± 4 (ε_{Ndi} = -0.8 ± 0.8). If instead we use in-run analytical errors (cf. Marks *et al.* 2004), the regression gives 1159 ± 34 Ma (MSWD = 3, n = 11) with $^{143}Nd/^{144}Nd_i$ = 0.51110 ± 3. To allow direct comparison with published data we also recalculate the regression and errors for the data of Marks *et al.* (2004) using the same protocol. This yields an age 1130 ± 130 Ma (MSWD = 2.9, Table 1) for their data, providing an age estimate that overlaps with other studies but with a significantly poorer precision than reported. Regression of the data from Paslick *et al.* (1993) gives an age consistent with the reported value of 1130 ± 50 Ma (MSWD = 0.08). In situ Nd isotopic analyses of eudialyte (Wu *et al.*, 2010) resulted in scattered values yielding an errorchron of 1128 ± 63 Ma (Table 1, Fig. 11). As such, we infer that our mineral – whole rock isochron age represents the most accurate and precise Sm-Nd age reported for the complex.

Individual outliers in the dataset, notably 535020-wr, are consistent with data which record minor isotopic disturbance by late-stage hydrothermal alteration. Such disturbance would be most pronounced in eudialyte-rich samples, as eudialyte exerts a strong control on the whole rock Sm and Nd budget. If we assume that whole rock Sm-Nd budgets are controlled by eudialyte, alkali feldspar and amphibole, a simple modal abundance calculation using the Sm-Nd concentrations (Supplementary Data Table S2) yields eudialyte proportions of *c.* 10%, 60% and 12%, in the black, red and white layers of Unit 0, respectively. For the

black and white kakortokite, these values are in good agreement with petrographic estimates. For the red kakortokite, however, 60% modal eudialyte is above our petrographic estimate (c. 40%). This implies a significant contribution to the bulk REE budget from other REE-phases, most likely rinkite (a REE-Ti-bearing disilicate). Rinkite contains c. 25 wt% RE_2O_3 and also interacts with late-stage fluids to produce secondary mineral assemblages (Rønsbo *et al.*, 2014). Subsolidus alteration of these phases may account for the minor discordance of the red kakortokite (535020-wr), suggesting that the fluids were capable of remobilizing REE. However, the isotopic compositions of the black and white whole rocks are undisturbed, even though they were subjected to the same alteration as the red kakortokite (Fig. 3). From this, we infer that the REE mobilizing capacity of the fluids was relatively low and that the circulating fluids were had a magmatic Nd isotopic signature. These inferences are supported by recent work on the Nd signatures of fresh and altered eudialyte (Van de Ven, 2018). Overall, the homogeneous Sm-Nd systematics of Ilímaussaq support the conclusion of Marks *et al* (2004) that the Sm-Nd system behaved as essentially a closed system during crystallization and cooling.

6.3 Rb-Sr systematics

Rb-Sr isotope data are strongly discordant and both whole rocks and mineral separates fail to yield isochron ages. The feldspar records the most disturbed signatures and their relatively unradiogenic Sr ratios with respect to their Rb/Sr ratios suggest significant loss of ^{87}Sr after crystallization. The 'young' feldspars weigh heavily on the best-fit regression through all samples, resulting in such significant scatter on the errorchron (MSWD=10737) that no meaningful interpretation is possible. Perthite is particularly sensitive to sub-solidus structural changes driven by exsolution and textural coarsening, both of which are accelerated by aqueous fluids (e.g. Parsons, 1978). In the kakortokite, the feldspar is microcline microperthite, which has been almost fully recrystallised into a patch perthite by

solution/reprecipitation (cf. Parsons 1978). The recrystallisation of feldspar at low (~400 C) temperatures allows exchange of Sr and Rb with the hydrothermal fluid and significantly influences the Rb-Sr system (e.g. Patchett *et al.*, 1979; Brooks *et al.*, 1986; Parsons *et al.*, 1988; Villa and Hanchar, 2013). Turbidity in the albitic component of the perthite laths (Fig. 3) has been attributed to fluid-induced microporosity, which allows the feldspar to be permeable to low temperature fluids. The consequence of these observations is that feldspar may have been open to Rb and Sr diffusion and loss for much longer periods than the low Rb/Sr phases.

Moorbath *et al.* (1960) previously reported anomalously young Rb-Sr ages around 1086 ± 24 Ma from three pegmatitic polylithionite samples with comparably high Rb/Sr ratios. The polylithionite data are shown together with other reported Rb-Sr data in Fig. 9 (recalculated from Table 1 in Moorbath *et al.*, 1960). The three points plot just below the 1091 Ma alkali feldspar trend, and together fall on a 3-point errorchron of 1106 ± 270 Ma (MSWD=20, assuming 2σ errors of 0.5% on $^{87}Rb/^{86}Sr$ and 0.05% on $^{87}Sr/^{86}Sr$) with a negative initial ratio (-0.2 ± 5.9). The large error and negative $^{87}Sr/^{86}Sr_i$ indicate considerable isotopic disequilibrium and loss of ^{87}Sr, as observed for the feldspars.

In contrast, the lower Rb/Sr samples (i.e. arfvedsonite, eudialyte and whole rocks, n = 9) define an errorchron trend of 1237 ± 21 Ma with excessive scatter (MSWD = 9811). One possible explanation for their radiogenic signatures is that they incorporated radiogenic Sr released from the alkali feldspar and other high Rb/Sr phases, analogous to Rb-Sr isotopic exchange between deuterically altered alkali feldspars and plagioclase (Brooks, 1968). However, analyzed whole rocks also plot above the 1160 Ma reference line and it appears that Rb-Sr isotopic exchange was not balanced on a whole-rock scale. This suggests an overall open system with a relative enrichment in ^{87}Sr.

Further evidence for open behaviour in the Rb-Sr system is provided from whole rock XRF data from the layered kakortokites sequence (Fig. 10; data from Bailey *et al.*, 2001). These show a significant enrichment in Sr concentrations between Units 0 and +3, reaching a ten-fold relative enrichment in the black kakortokite of Unit 3 (from *c.* 100 to 1250 ppm Sr). The peak in Sr concentrations is inconsistent with fractional crystallization or cumulate processes, and strongly suggests remobilization by internally and/or externally derived hydrothermal fluids enriched in Sr. Local subsolidus Sr enrichment, possibly by external fluids, was inferred from gittinsite-bearing ($CaZrSi_2O_7$) eudialyte alteration assemblages containing mantles of Sr-rich secondary eudialyte (Borst *et al.*, 2016). Potential external sources for Sr include (1) seawater entering the complex along faults, as proposed by Graser and Markl (2008), or (2) preferential leaching of radiogenic Sr from the granitic Ketilidian basement, as suggested by Blaxland *et al.* (1976b).

Irrespective of the nature of the disturbance, the data support the notion that Rb and Sr are highly mobile and that the Rb-Sr system is an unreliable chronometer for agpaitic (or peralkaline) rocks (e.g. Krumrei *et al.*, 2006; Marks *et al.*, 2003). Therefore, it is fortuitous that the reported (and commonly cited) Rb-Sr ages by Waight *et al.* (2002) and Blaxland *et al.* (1976b) were consistent with the baddeleyite/zircon U-Pb ages and the new $^{40}Ar/^{39}Ar$ age. However, both ages were calculated with different decay constants for ^{87}Rb (Table 1). When using the revised decay constant of 1.397×10^{-11} a^{-1} (Villa *et al.*, 2015a) the 2-point Rb-Sr age of Waight *et al.* (1160 ± 2 Ma) changes to 1179 ± 2 Ma (Table 1). A new regression of Blaxland's data (agpaites only) yields 1162 ± 21 Ma with MSWD=53 instead of 3.6, which renders this an errorchron. In summary, all studies demonstrate chemical opening of the Rb-Sr system and so other isotopic systems will provide more accurate dating of agpaitic rocks.

6.4 $^{40}Ar/^{39}Ar$ AGES

Four single-crystal $^{40}Ar/^{39}Ar$ step-heating experiments of black kakortokite amphibole yield two plateau ages. Only one of these is robust with an age of 1156.6 ± 1.4 Ma (MSWD=1.5) for 5 consecutive steps comprising >99% of the total ^{39}Ar released. The second 'plateau' age is within error of the former (Supplementary Table S4), but is associated with a MSWD value of >2 and comprises only 47% of total ^{39}Ar released, suggesting geological disturbance of the K-Ar system in this amphibole crystal. We interpret the young ages of the first heating steps for all grains, associated with low % $^{40}Ar^*$ and higher Ca/K, to be due to minor alteration products or loosely adhered argon with an extraneous ^{40}Ar component. Slight variations in the gas release patterns as a function of laser power can be attributed to natural compositional variation and zoning in the Ca/(K+Na) ratios of the amphiboles (e.g. Pfaff *et al.*, 2008), which influences their degassing behaviour (Dahl, 1996; Villa *et al.*, 2000; Krumrei *et al.*, 2006). The high Ca/K signatures of the final heating steps may reflect gas release from more Ca-enriched amphibole domains (cores) with higher degassing temperatures, or alternatively, from micro-inclusions of primary magmatic Ca-rich phases such as apatite or fluorite in arfvedsonite (Fig. 3c). Either way, the high Ca/K ratios are not associated with significantly different calculated plateau ages.

While the closure temperature for Ar in sodic amphiboles is relatively low (c. 500-550 °C), taking into account the ionic porosity (Dahl *et al.*, 1996), the solidus temperature for agpaitic melts is possibly lower (c. 500-450 °C; e.g. Markl *et al.* 2001). Arfvedsonite is among the first phases to crystallize (c. 700-550 °C), and so the $^{40}Ar/^{39}Ar$ ratio may modify prior to full crystallisation of the melt. Since the complex has experienced no significant metamorphic overprinting since emplacement, the amphibole plateau age are interpreted as a crystallization age. Fluid assisted re-equilibration at lower temperatures (c. 450-350 °C), associated with the formation of secondary aegirine and possibly partial loss of argon, may

have occurred after crystallization. This can readily account for the disturbance in the $^{40}Ar/^{39}Ar$ gas release patterns for two of the grains.

$^{40}Ar/^{39}Ar$ data presented by Krumrei *et al.* (2006) were derived from furnace step-heating experiments on multi-grain amphibole aliquots (c. 10 mg) from intrusive units in the complex. Using modern values for the K decay constant and the FCT monitor age (i.e. Min *et al.*, 2000; Rivera *et al.*, 2011), their $^{40}Ar/^{39}Ar$ data yield ages between 1150.5 and 1161.2 Ma (Table 1), i.e. within external error of our new plateau age. However, close examination of their data shows that the plateaus are relatively poorly defined, i.e. MSWD values are too high (Table 1) and released ^{39}Ar fractions too low to yield acceptable plateau ages, as pointed out by Baksi (2007). Because the experiments of Krumrei *et al.* (2006) were run as multi-grain step-heating experiments using a furnace, the non-plateau ages could reflect mixing of variably isotopically disturbed grains. The presence of isotopically disturbed grains is clearly demonstrated in our single crystal step-heating approach, which allows recognition and therefore exclusion of such grains.

6.5 Comparison of Geochronological Techniques

A compilation of geochronological data from the literature and the present study is given in Table 1, along with associated MSWD, initial ratios and decay constants used. The kakortokite isotopic data reveal variable degrees of isotopic disturbance in all radiogenic systems (Fig. 11). This is most evident in the Rb-Sr system, which yields geologically meaningless ages with low precision, accuracy and ill-defined initial ratios. The Rb-Sr system records extensive open system behavior demonstrated in all minerals, and so is of limited suitability for dating agpaitic rocks. The Sm-Nd system is less susceptible to isotopic disturbance by late-stage hydrothermal fluids, although some scatter in the data can be explained by this process. The Sm-Nd isochron ages, however, are associated with large uncertainties (low precision, Fig 11), which in part is due to the narrow spread in Sm/Nd

ratios of Ilímaussaq rocks and minerals. The Sm-Nd isochron method may thus provide tighter age constraints for agpaitic rocks and minerals that display a wider range in REE ratios, providing that a closed-system fluid evolution can be demonstrated. The U-Pb system demonstrates minor isotopic disturbance in two arfvedsonite and one feldspar separates. Exclusion of these samples nevertheless provides a relatively precise ^{235}U-^{207}Pb whole rock-mineral isochron age of 1168.5 ± 8.8 Ma. This is within error of the U/Pb baddeleyite age from the earliest intrusive phase (Fig. 11) and is considered the most precise non-single mineral age estimate for the agpaitic units.

Still higher precision constraints are obtained from single crystal $^{40}Ar/^{39}Ar$ dating of sodic amphiboles. The step-heating approach provides a self-filtering mechanism for the effects of alteration and late-stage isotopic re-equilibration. As such, the new single crystal amphibole $^{40}Ar/^{39}Ar$ plateau age of 1156 ± 1.4 Ma is put forward as the most precise age for the agpaitic units of Ilímaussaq to date (Fig. 11). However, this age quotes internal analytical errors only and if we consider uncertainties related to the accuracy and precision of the FCT age and decay constants we obtain an external error of ± 7.7 Ma (0.66%) on the plateau age (bracketed values in Table 1). The use of different FCT values produces ages within analytical error (Table 1), and so the uncertainty expressed by the external error mainly relates to error associated with the decay constant. Taking this into account, the $^{40}Ar/^{39}Ar$ single mineral age approaches the level of precision of that obtained by the ^{235}U-^{207}Pb whole rock-mineral isochron age. Hence, both techniques are suitable for dating agpaitic rocks but neither provide the required precision or accuracy to resolve internal age differences between non-agpaitic and agpaitic units at Ilímaussaq. A combination of single crystal $^{40}Ar/^{39}Ar$ dating and U-Pb whole rock mineral isochron dating could provide valuable age and longevity constraints for agpaitic complexes that experienced more prolonged emplacement and cooling histories, or metamorphism after emplacement (e.g. Sushina Hill, Norra Kärr).

6.6 PETROGENETIC CONSTRAINTS

The data also provide an opportunity to revisit the petrogenesis of the agpaitic magmas at Ilímaussaq in relation to other Gardar intrusions. The Ilímaussaq melts are described as residual liquids from a mantle-derived transitional basaltic magma that experienced extensive fractional crystallization in deeper level magma chambers, along with low degrees of crustal contamination prior to emplacement in the shallow crust (Larsen and Sørensen, 1987; Stevenson, 1997; Marks *et al.*, 2004). Sr-Nd isotope systematics of the kakortokite and other Ilímaussaq units are shown in Fig. 12, illustrating a narrow range in ε_{Ndi} values (0 to -2) combined with highly variable $^{87}Sr/^{86}Sr_i$ (0.68 to 0.72). Other Gardar isotopic data are plotted for comparison, including relatively primitive magmas of the Brown dykes (*c.* 1280 Ma; Bartels *et al.*, 2015), Eriksfjord basalts (*c.* 1200 Ma; Halama *et al.*, 2003), Isortôq dykes (*c.* 1190 Ma; Halama *et al.*, 2004), basalts and lamprophyres from the Ivigtût area (*c.* 1280 Ma; Goodenough *et al.*, 2002), as well as lamprophyres, phonolites/syenites and carbonatites from Qassiarsuk (*c.* 1200 Ma; Andersen, 1997), Grønnedal-Ika (c. 1290 Ma; Nd data from Halama *et al.*, 2005 and Sr data from Taubald *et al.*, 2004) and the Igaliko area (*c.* 1150 Ma; Pearce and Leng, 1996). Primitive Gardar magmas typically show mantle-derived signatures with positive ε_{Ndi} >1 and $^{87s}Sr/^{86}Sr_i$ of *c.* 0.702-0.703 close to Bulk Silicate Earth. Trends towards lower ε_{Ndi} < 0 and more radiogenic $^{87}Sr/^{86}Sr_i$ (up to 0.705) have been explained by variable degrees of bulk contamination by Archaean and Proterozoic (Ketilidian) crustal material (e.g. Andersen, 1997; Goodenough *et al.*, 2000; 2002; Halama *et al.*, 2004; Marks *et al.*, 2003; Bartels *et al.*, 2015; evolution curves 3a and 3b in Fig. 12). Some of the lowest Gardar ε_{Ndi} values (-11) are measured in the gabbroic-syenitic Isortôq dykes, where AFC modelling suggested a maximum of 10% contamination with Archaean granulite-facies lower crust (Halama *et al.*, 2004).

Relative to other Gardar complexes, the Ilímaussaq melts show a wide range in $^{87}Sr/^{86}Sr_i$ in combination with a narrow range of sub-chondritic ε_{Ndi}. Although initial $^{87}Sr/^{86}Sr$ are less well constrained than ε_{Ndi} (a consequence of the high Rb/Sr and large age correction error extrapolation), calculated $^{87}Sr/^{86}Sr_i$ for the agpaites are much higher (0.7096 ± 0.0022) than for the augite syenite (c. 0.703 ± 0.002, Blaxland *et al.*, 1976b). Initial $^{87}Sr/^{86}Sr$ for the lujavrite are even higher (up to 0.72, Fig. 12, Blaxland *et al.*, 1976b), while our kakortokite Rb-Sr isochron yields an intermediate initial of 0.707 ± 0.003. Given the large uncertainty on this value, calculated $^{87}Sr/^{86}Sr_i$ for individual eudialyte separates potentially provide tighter constraints for the initial Sr composition of the kakortokite melt because of their low Rb/Sr ratios. The eudialyte initials (0.7055-0.7088 ± 0.0004, red diamonds in Fig. 12) are an order of magnitude more precise than the $^{87}Sr/^{86}Sr_i$ obtained from the isochron (black diamond in Fig. 12), however, individual values do not overlap within error. This again indicates isotopic disequilibrium, and so the Sr initial of the kakortokite melt remains poorly constrained. Nevertheless, the data is consistent with an overall evolution of increasingly radiogenic $^{87}Sr/^{86}Sr_i$ from *c.* 0.703 in the augite syenite, to c. 0.707 in the kakortokite, and 0.721 in the most evolved lujavrites, while maintaining a narrow range of ε_{Ndi} (c. 0.5 to -1.5).

Blaxland *et al.* (1976b) explained the increase in $^{87}Sr/^{86}Sr_i$ in progressive melts to selective enrichment of ^{87}Sr by leaching of radiogenic Sr from unstable positions in Rb lattices sites from feldspars in the Ketilidian crust (evolution curve 1, Fig. 12). A similar process of preferential ^{87}Sr uptake from country rock, most likely by magmatic hydrothermal fluids, was invoked to explain high $^{87}Sr/^{86}Sr_i$ values (up to 0.72) from other Gardar complexes such as Ivigtut, North Qoroq, Grønnedal-Ika and North Motzfeldt (Blaxland, 1976a; Finch *et al.*, 2001; Goodenough *et al.*, 2000; Taubald *et al.*, 2004). Taubald *et al.* (2004) also noted significant heterogeneities in $^{87}Sr/^{86}Sr_i$ values between silicic and carbonate phases in a

silicocarbonate from Grønnedal-Ika, and explained this by preferential uptake of ^{87}Sr and Rb into the silicate phase during carbonate-silicate immiscibility.

For the Ilímaussaq melts, Stevenson *et al.* (1997) argued that bulk assimilation of Ketilidian crust could explain the observed trends towards high Sr ratios and slightly negative ε_{Ndi} values, following assimilation-fractional crystallization (AFC) of a basaltic, to augite syenitic, to agpaitic melt that assimilated Ketilidian crust at decreasing rates (evolution curve 2, Fig. 12). The fact that ε_{Ndi} remains stable with continued assimilation is due to the high Nd (> 100 ppm) and low Sr contents (< 150 ppm) in the agpaitic melts, relative to low Nd (~35 ppm) and high Sr (~600 ppm) contents of the contaminant. Following the AFC calculations of Stevenson *et al.* ε_{Ndi} values decrease from ~2 (basaltic melt), to ~0 (augite syenite) and then to ~ -1 (lujavrite), while $^{87}Sr/^{86}Sr_i$ increases from 0.702 to 0.709, with gradually decreasing rates of assimilation relative to fractional crystallization. The lujavrite stage was modelled by 17% of crustal assimilation after at least 85% fractional crystallization of the augite syenite melt. Using higher assimilation/crystallization rates for the alkali granite, 40% bulk contamination would be required to yield ε_{Ndi} of -1 to -2 (Stevenson *et al.* 1997). Marks *et al.* (2004) later calculated that 13% of contamination with Archaean lower crust during storage and/or ascent of the augite syenitic melt would be sufficient to explain both Si-saturation and low ε_{Ndi} (-3.1) of the alkali granite (Fig. 8). The authors noted that greater amounts of upper crustal contamination was unlikely, due to the uniform $\delta^{18}O$ values (+5.2 to 5.7‰) for the alkali granite and other Ilímaussaq melts. Although this model did not consider Sr isotopes, 13% of lower crustal input can be considered a maximum estimate of contamination for all Ilímaussaq melts. Few samples that yielded ε_{Ndi} values down to -5.7 for lujavrites and augite syenites (Fig. 8, 12) derived from the margin of the complex, however, can be explained by local assimilation of Ketilidian crust during emplacement (Stevenson *et al.*, 1997).

An integrated study of Nd-Sr isotopes of mineral separates from all units, as performed in the present study, ideally with the addition of stable isotopic data, could help to differentiate between proposed petrogenetic processes and constrain the extent of contamination through (i) preferential leaching of radiogenic ^{87}Sr during ascent and emplacement, (ii) crustal assimilation/fractional crystallization during ascent, (iii) crustal contamination along the margins of the complex and (iv) post-magmatic hydrothermal activity. A detailed understanding of these processes is essential to unravelling the isotopic complexity of these economically important rock types.

CONCLUSIONS

Rb/Sr, U/Pb, Rb/Sr and Ar/Ar isotopic data are presented for whole rocks and mineral separates (eudialyte, arfvedsonite amphibole & alkali feldspar) from a single co-genetic kakortokite unit in the Ilímaussaq complex. New geochronological data are presented and compared to published ages for the complex. The applicability of traditional isochron methods for dating agpaitic rocks and challenges related to pervasive metasomatic alteration, affecting isotopic systems to different extents, have been discussed. The following conclusions are drawn based on the data presented:

I. Single-crystal amphibole $^{40}Ar/^{39}Ar$ step-heating experiments yield a plateau age of 1156.6 ± 1.4 Ma (MSWD=1.5, p=0.2), the most precise crystallization age for the agpaitic units of the Ilímaussaq complex currently available. The external error imposed by uncertainties on the geochronological constants is ± 7.7 Ma.

II. Whole rock, eudialyte and feldspar data from kakortokite unit 0 yield well-defined ^{207}Pb-^{206}Pb and ^{235}U-^{207}Pb isochron ages of 1159 ± 17 Ma (MSWD=0.96) and 1168.5 ± 8.8 Ma (MSWD=0.82), respectively. Both are consistent with reported baddeleyite and zircon U-Pb ages from the earlier intrusive units, as well as the new

kakortokite $^{39}Ar/^{40}Ar$ amphibole data. Although some chemical disturbance is recorded for U, the U-Pb system appears relatively robust to late-magmatic peralkaline fluid activity. The U-Pb isochron method thus provides reasonable first order age constraints for agpaitic rocks when single mineral dating techniques are not available.

III. Sm-Nd isotope data yield a kakortokite isochron of 1156 ± 53 Ma (MSWD=0.23) with $^{143}Nd/^{144}Nd_i$ of 0.511103 ± 39, corresponding to ε_{Ndi} = -0.8 ± 0.8. The kakortokite minerals and whole rocks show significantly less scatter around the isochron than published Sm-Nd data for the complex, reflecting their origin from a single co-genetic unit. Minor discordancy of some samples is attributed to isotopic disturbance by late-magmatic alteration. However, initial ratios are indistinguishable within error, suggesting that the impact of alteration on the Sm-Nd system was minor and that the fluids had a magmatic Nd signature. A compilation of Nd data demonstrate that most Ilímaussaq melts are characterized by a narrow subchondritic range of initial ε_{Ndi} values between -0.2 and -1.2.

IV. Rb-Sr isotope systematics in the kakortokite reveal significant chemical disturbance and render no reliable age information. Alkali feldspars define a 3-point errorchron of 1106 ± 94 Ma, MSWD=25, plotting well below the 1160 Ma trend and suggesting significant loss of ^{87}Sr after crystallization. Whole rocks, as well as eudialyte and amphibole separates (low Rb/Sr) plot above a 1160 Ma reference line and define an anomalously old errorchron trend of 1237 ± 21 Ma with significant geological scatter (MSWD>900). This suggests extensive open-system behavior and an overall enrichment in radiogenic ^{87}Sr.

V. Initial Sr compositions calculated from eudialyte separates (low Rb/Sr) provide the most precise constraints for the initial Sr isotopic composition of the kakortokite

melt, although variations between the individual samples indicate isotopic disequilibrium. The marked overall increase in $^{87}Sr/^{86}Sr_i$ from the earliest intrusive units (0.703) to the agpaitic units (c. 0.707), combined with the narrow range of sub-chondritic ε_{Ndi} can be explained by minor crustal assimilation and preferential leaching of ^{87}Sr from the Proterozoic basement during emplacement and cooling of the complex.

ACKNOWLEDGEMENTS

This work is published with permission of the Geological Survey of Denmark and Greenland. We thank Olga Nielsen, Michael Nielsen, Mojagan Alaei, Toni Larsen, Toby Leeper, Martin Heckscher, Tonny Bernt Thomsen and Cristina Jensen de Olsen for their help with sample preparation and lab procedures, and Per Kalvig for management of the GreenCrimi project. This research was funded by the Carlsberg Fund [grant nr. 2013_01_0191 to TW] and Geocenter Denmark [GreenCrimi project, grant nr. 4-2012 to AMB]. Quadlab is funded by a grant from the Villum Foundation to MS. AMB and AF thank the NERC SoS RARE project [grant nr. NE/M011429/1] for support during the writing of this manuscript.

REFERENCES

Aldrich, L., Wetherill, G., Tilton, G., Davis, G., 1956. Half-life of Rb^{87}. Physical Review 103, 1045.

Andersen, S., Bohse, H., Steenfelt, A., 1988. Geological map 1:20 000, The southern part of the Ilímaussaq complex, South Greenland Grønlands Geologiske Undersøgelse & Geodætisk Institut Denmark, Archive nr. 60V3183.

Andersen, T., 1997. Age and petrogenesis of the Qassiarsuk carbonatite-alkaline silicate volcanic complex in the Gardar rift, South Greenland. Mineralogical Magazine 61, 499-513.

Bailey, J.C., Gwozdz, R., Rose-Hansen, J., Sørensen, H., 2001. Geochemical overview of the Ilímaussaq alkaline complex, South Greenland. Geological Survey of Denmark and Greenland Bulletin 190, 20.

Baksi, A. K., 2007. Comment on "A 40Ar/39Ar and U/Pb isotopic study of the Ilímaussaq complex, South Greenland: Implications for the 40K decay constant and the duration of magmatic activity in a peralkaline complex" by Krumrei *et al.*. Chemical Geology 244, 344-346.

Bartels, A., Nielsen, T.F., Lee, S.R., Upton, B.G., 2015. Petrological and geochemical characteristics of Mesoproterozoic dyke swarms in the Gardar Province, South Greenland: Evidence for a major sub-continental lithospheric mantle component in the generation of the magmas. Mineralogical Magazine 79, 909-939.

Blaxland, A.B., 1976a. Rb-Sr isotopic evidence for the age and origin of the Ivigtut granite and associated cryolite body, South Greenland. Economic Geology 71, 864-869.

Blaxland, A.B., Van Breemen, O., Steenfelt, A., 1976b. Age and origin of agpaitic magmatism at Ilímaussaq, South Greenland: Rb-Sr study. Lithos 9, 31-38.

Blaxland, A. B., Van Breemen, O., Emeleus, C. H., Andersen, J. G., 1978. Age and origin of the major syenite centers in the Gardar province of south Greenland: Rb-Sr studies. Geological Society of America Bulletin 89, 231-244.

Bohse, H. and Andersen, S., 1981. Review of the stratigraphic divisions of the kakortokite and lujavrite in southern Ilímaussaq. Rapport Grønlands Geologisk Undersøgelse, 103, 9.

Bohse, H., Brooks, C.K., Kunzendorf, H., 1971. Field observations on the kakortokites of the Ilímaussaq intrusion, South Greenland, including mapping and analyses by

portable X-Ray fluorescence equipment for zirconium and niobium. Rapport Grønlands Geologisk Undersøgelse 38, 43.

Borst, A.M., Friis, H., Andersen, T., Waight, T.E. Nielsen, T.F.D., Smit M., 2016. Zirconosilicates in the kakortokites of the Ilímaussaq complex, South Greenland: Implications for fluid evolution and HFSE-REE mineralization in agpaitic systems, Mineralogical Magazine 80, 1-26.

Borst, A. M., Friis, H., Nielsen, T. F. D., Waight, T. E., 2018. Bulk and mush melt evolution in agpaitic intrusions: insights from compositional zoning in eudialyte, Ilímaussaq Complex, South Greenland. Journal of Petrology 59, 589-612.

Brooks, C., 1968. Relationship between feldspar alteration and the precise post-crystallization movement of rubidium and strontium isotopes in a granite. Journal of Geophysical Research 73, 4751-4757.

Cherniak, D. and Watson, E., 1992. A study of strontium diffusion in K-feldspar, Na-K feldspar and anorthite using Rutherford backscattering spectroscopy. Earth and Planetary Science Letters 113, 411-425.

Dahl, P. S., 1996. The effects of composition on retentivity of argon and oxygen in hornblende and related amphiboles: A field-tested empirical model. Geochimica et Cosmochimica Acta 60, 3687-3700.

DePaolo, D.J., 1981. Trace element and isotopic effects of combined wallrock assimilation and fractional crystallization. Earth and Planetary Science Letters 53, 189-202.

DePaolo, D.J., 1988. Neodymium isotope geochemistry: an introduction. Springer - Verslag, New York. Literature notes

Estrade, G., Béziat, D., Salvi, S., Tiepolo, M., Paquette, J.-L., Rakotovao, S., 2014. Unusual evolution of silica-under-and-oversaturated alkaline rocks in the Cenozoic

Ambohimirahavavy Complex (Madagascar): Mineralogical and geochemical evidence. Lithos 206, 361-383.

Finch, A., Goodenough, K., Salmon, H., Andersen, T. 2001. The petrology and petrogenesis of the North Motzfeldt centre, Gardar province, South Greenland. Mineralogical Magazine 65, 759-774

Ferguson, J., 1964. Geology of the Ilímaussaq alkaline intrusion, South Greenland. Description of map and structure. Meddelelser om Grønland, 712, 82.

Giletti, B.J., 1991. Rb and Sr diffusion in alkali feldspars, with implications for cooling histories of rocks. Geochimica et Cosmochimica Acta 55, 1331-1343.

Goldstein, S., O'Nions, R., Hamilton, P., 1984. A Sm-Nd isotopic study of atmospheric dusts and particulates from major river systems. Earth and Planetary Science Letters 70, 221-236.

Goodenough, K.M., Upton, B.G.J., Ellam, R.M., 2000. Geochemical evolution of the Ivigtut granite, South Greenland: a fluorine-rich "A-type" intrusion. Lithos 51, 205-221.

Goodenough, K.M., Upton, B.G.J., Ellam, R.M., 2002. Long-term memory of subduction processes in the lithospheric mantle: evidence from the geochemistry of basic dykes in the Gardar Province of South Greenland. Journal of the Geological Society 159, 705-714.

Graser, G. and Markl, G., 2008, Ca-rich ilvaite–epidote–hydrogarnet endoskarns: A record of late-magmatic fluid influx into the persodic Ilímaussaq complex, South Greenland. Journal of Petrology, 49, 239-265.

Halama, R., Wenzel, T., Upton, B., Siebel, W., Markl, G., 2003. A geochemical and Sr-Nd-O isotopic study of the Proterozoic Eriksfjord Basalts, Gardar Province, South

Greenland: Reconstruction of an OIB signature in crustally contaminated rift-related basalts. Mineralogical Magazine 67, 831-853.

Halama, R., Marks, M., Brügmann, G., Siebel, W., Wenzel, T., Markl, G., 2004. Crustal contamination of mafic magmas: evidence from a petrological, geochemical and Sr–Nd–Os–O isotopic study of the Proterozoic Isortoq dike swarm, South Greenland. Lithos 74, 199-232.

Halama, R., Vennemann, T., Siebel, W., Markl, G., 2005. The Grønnedal-Ika carbonatite–syenite complex, South Greenland: carbonatite formation by liquid immiscibility. Journal of Petrology 46, 191-217.

Hunt, E. J., Finch, A. A., Donaldson, C. H., 2017. Layering in peralkaline magmas, Ilímaussaq Complex, S Greenland, Lithos 268–271:1-15.

Jacobsen, S.B. and Wasserburg, G., 1980. Sm-Nd isotopic evolution of chondrites. Earth and Planetary Science Letters, 50, 139-155.

Kogarko, L. N., 1974. Role of volatiles. In: Sørensen, H. (ed.) The alkaline rocks. London: Wiley, Chapter 4.4, p. 474-487.

Konnerup-Madsen, J. and Rose-Hansen, J., 1984, Composition and significance of fluid inclusions in the Ilímaussaq peralkaline granite, South Greenland. Schweizerische Mineralogische und Petrographische Mitteilungen 107, 317-326.

Kramm, U. and Kogarko, L. N., 1994, Nd and Sr isotope signatures of the Khibina and Lovozero agpaitic centres, Kola Alkaline province, Russia. Lithos 32, 225-242.

Krumrei, T.V., Villa, I.M., Marks, M.A.W., Markl, G., 2006. A $^{40}Ar/^{39}Ar$ and U/Pb isotopic study of the Ilímaussaq complex, South Greenland: Implications for the ^{40}K decay constant and for the duration of magmatic activity in a peralkaline complex. Chemical Geology 227, 258-273.

Kuiper, K. F., Deino, A., Hilgen, F. J., Krijgsman, W., Renne, P. R., Wijbrans, J. R., 2008. Synchronizing the rock clocks of Earth history. Science 320, 500–504.

Larsen, L.M. and Sørensen, H., 1987. The Ilímaussaq intrusion—progressive crystallization and formation of layering in an agpaitic magma. Geological Society, London, Special Publications, 30, 473-488.

Liew, T.C., Hofmann, A.W., 1988. Precambrian crustal components, plutonic associations, plate environment of the Hercynian Fold Belt of central Europe: indications from a Nd and Sr isotopic study. Contributions to Mineralogy and Petrology 98, 129-138.

Ludwig, K., 2003. Using Isoplot/Ex, Version 3. A Geochronological Toolkit for Microsoft Excel. Berkeley Geochronology Center Special Publication 4.

Lugmair, G.W. and Marti, K, 1978. Lunar initial 143Nd/144Nd: Differential evolution of the lunar crust and mantle. Earth and Planetary Science Letters, 39, 349-357.

Markl, G. and Baumgartner, L., 2002. pH changes in peralkaline late-stage fluids. Contributions to Mineralogy and Petrology 144, 331-346.

Markl, G., Marks, M. A. W., Frost, B. R., 2010. On the controls of oxygen fugacity in the generation and crystallization of peralkaline melts. Journal of Petrology 51, 1831-1847.

Marks, M., Vennemann, T., Siebel, W., Markl, G., 2003. Quantification of Magmatic and Hydrothermal Processes in a Peralkaline Syenite–Alkali Granite Complex Based on Textures, Phase Equilibria, and Stable and Radiogenic Isotopes. Journal of Petrology 44, 1247-1280.

Marks, M.A.W., Vennemann, T., Siebel, W., Markl, G., 2004. Nd-, O-, and H-isotopic evidence for complex, closed-system fluid evolution of the peralkaline Ilímaussaq intrusion, South Greenland. Geochimica et Cosmochimica Acta 68, 3379-3395.

Marks, M.A.W., Hettmann, K., Schilling, J., Frost, B.R., Markl, G., 2011. The Mineralogical diversity of alkaline igneous rocks: critical factors for the transition from miaskitic to agpaitic phase assemblages. Journal of Petrology 52, 439-455.

Marks, M.A.W. and Markl, G., 2015. The Ilímaussaq alkaline complex, South Greenland, In: Charlier, B., Namur, O., Latypov, R., Tegner, C. (eds.) Layered Intrusions. Springer, 649-691.

Marks, M.A.W. and Markl, G., 2017. Global review on agpaitic rocks. Earth-Science Reviews 173, 229-258

McCreath, J. A., Finch, A. A., Simonsen, S. L., Donaldson, C. H., Armour-Brown, A., 2012. Independent ages of magmatic and hydrothermal activity in alkaline igneous rocks: The Motzfeldt Centre, Gardar Province, South Greenland. Contributions to Mineralogy and Petrology 163, 967-982.

Min, K., Mundil, R., Renne, P.R., Ludwig, K.R., 2000. A test for systematic errors in $^{40}Ar/^{39}Ar$ geochronology through comparison with U/Pb analysis of a 1.1-Ga rhyolite. Geochimica et Cosmochimica Acta 64, 73-98.

Mitchell, R. H. and Liferovich, R. P., 2006. Subsolidus deuteric/hydrothermal alteration of eudialyte in lujavrite from the Pilansberg alkaline complex, South Africa. Lithos 91, 352-372.

Moorbath, S., Webster, R., Morgan, J., 1960. Absolute age determination in South-West Greenland: The Julianehåb Granite, the Ilímaussaq Batholith and the Kûngnât Syenite Complex. Meddelelser om Grønland. 162-9. 1-13.

Möller, V. and Williams-Jones, A. E., 2016. Stable and radiogenic isotope constraints on the magmatic and hydrothermal evolution of the Nechalacho Layered Suite, northwest Canada. Chemical Geology 440, 248-274.

Parsons, I., 1978. Feldspars and fluids in cooling plutons. Mineral Magazine, 42, 1-17.

Parsons, I., Rex, D., Guise, P., Halliday, A., 1988. Argon-loss by alkali feldspars. Geochimica et Cosmochimica Acta 52, 1097-1112.

Paslick, C.R., Halliday, A.N., Davies, G.R., Mezger, K., Upton, B., 1993. Timing of Proterozoic magmatism in the Gardar Province, southern Greenland. Geological Society of America Bulletin 105, 272-278.

Patchett, P., Van Breemen, O., Martin, R., 1979. Sr isotopes and the structural state of feldspars as indicators of post-magmatic hydrothermal activity in continental dolerites. Contributions to Mineralogy and Petrology 69, 65-73.

Pearce, N.J.G., Leng, M.J., 1996. The origin of carbonatites and related rocks from the Igaliko Dyke Swarm, Gardar Province, South Greenland: field, geochemical and C-O-Sr-Nd isotope evidence. Lithos 39, 21-40.

Pfaff, K., Krumrei, T., Marks, M., Wenzel, T., Rudolf, T., Markl, G., 2008. Chemical and physical evolution of the 'lower layered sequence' from the nepheline syenitic Ilímaussaq intrusion, South Greenland: Implications for the origin of magmatic layering in peralkaline felsic liquids. Lithos 106, 280-296.

Ratschbacher, B.C., Marks, M.A.W., Bons, P.D., Wenzel, T., Markl, G., 2015. Emplacement and geochemical evolution of highly evolved syenites investigated by a combined structural and geochemical field study: The lujavrites of the Ilímaussaq complex, SW Greenland. Lithos 231, 62-76.Renne, P.R., Swisher, C.C., Deino, A.L., Karner, D.B., Owens, T.L. and DePaolo, D.J., 1998, Intercalibration of standards, absolute ages and uncertainties in $^{40}Ar/^{39}Ar$ dating. Chemical Geology, 145, 117-152.

Renne, P.R., Mundil, R., Balco, G., Min, K., Ludwig, K.R., 2010. Joint determination of ^{40}K decay constants and $^{40}Ar*/^{40}K$ for the Fish Canyon sanidine standard, and improved accuracy for $^{40}Ar/^{39}Ar$ geochronology. Geochimica et Cosmochimica Acta 74, 5349-5367.

Renne, P.R., Balco, G., Ludwig, K.R., Mundil, R., Min, K., 2011. Response to the comment by W.H. Schwarz *et al.* On "joint determination of ^{40}K decay constants and ^{40}Ar∗/^{40}K for the Fish Canyon sanidine standard, and improved accuracy for ^{40}Ar/^{39}Ar geochronology" by P.R. Renne *et al.* (2010). Geochimica et Cosmochimica Acta, 75, 5097-5100.

Rivera, T.A., Storey, M., Zeeden, C., Hilgen, F.J., Kuiper, K., 2011. A refined astronomically calibrated ^{40}Ar/^{39}Ar age for Fish Canyon sanidine. Earth and Planetary Science Letters, 311, 420-426.

Rønsbo, J.G., Sørensen, H., Roda-Robles, E., Fontan, F., Monchoux, P., 2014. Rinkite–nacareniobsite-(Ce) solid solution series and hainite from the Ilímaussaq alkaline complex: occurrence and compositional variation. Bulletin of the Geological Society of Denmark 62, 1-15.

Schwarz, W.H., Kossert, K., Trieloff, M., Hopp, J., 2011. Comment on the "Joint determination of ^{40}K decay constants and ^{40}Ar∗/^{40}K for the Fish Canyon Sanidine standard, and improved accuracy for ^{40}Ar/^{39}Ar geochronology" by P.R. Renne *et al.* 2010. Geochimica et Cosmochimica Acta, 75, 5094-5096.

Scott, J. M., Waight, T. E., van der Meer, Q. H. A., Palin, J. M., Cooper, A. F., Münker, C., 2014. Metasomatized ancient lithospheric mantle beneath the young Zealandia microcontinent and its role in HIMU- like intraplate magmatism. Geochemistry, Geophysics, Geosystems 15, 3477-3501.

Siebel, W., Reitter, E., Wenzel, T., Blaha, U., 2005. Sr isotope systematics of K-feldspars in plutonic rocks revealed by the Rb–Sr microdrilling technique. Chemical Geology 222, 183-199.

Sjöqvist, A. S. L., Cornell, D. H., Andersen, T., Christensson, U. I., Berg, J. T., 2017. Magmatic age of rare-earth element and zirconium mineralization at the Norra Kärr

alkaline complex, southern Sweden, determined by U–Pb and Lu–Hf isotope analyses of metasomatic zircon and eudialyte. Lithos 294-295, 73-86.

Steiger, R.H. and Jäger, E., 1977. Subcommission on geochronology: convention on the use of decay constants in geo-and cosmochronology. Earth and Planetary Science Letters 36, 359-362.

Stevenson, R., Upton, B.G.J., Steenfelt, A., 1997. Crust-mantle interaction in the evolution of the Ilímaussaq Complex, South Greenland: Nd isotopic studies. Lithos 40, 189-202.

Sørensen, H., 1992. Agpaitic nepheline syenites: a potential source of rare elements. Applied Geochemistry 7, 417-427.

Sørensen, H., 1997. The agpaitic rocks; an overview. Mineralogical Magazine 61, 485-498.

Sørensen, H., Bohse, H., Bailey, J.C., 2006. The origin and mode of emplacement of lujavrites in the Ilímaussaq alkaline complex, South Greenland. Lithos 91, 286-300.

Taubald, H., Morteani, G. & Satir, M. (2004). Geochemical and isotopic (Sr, C, O) data from the alkaline complex of Grønnedal-Íka (South Greenland): evidence for unmixing and crustal contamination. International Journal of Earth Sciences 93, 348-360.

Upton, B.G.J., 2013. Uniqueness of the southern branch of the Gardar rift. Geol. Surv. Den. Greenl. Bull. 29, pp. 1-124.

Upton, B.G.J. and Emeleus, C.H., 1987. Mid-Proterozoic alkaline magmatism in southern Greenland: the Gardar province. Geological Society, London, Special Publications 30, 449-471.

Upton, B., Emeleus, C., Heaman, L., Goodenough, K., Finch, A., 2003. Magmatism of the mid-Proterozoic Gardar Province, South Greenland: chronology, petrogenesis and geological setting. Lithos 68, 43-65.

Ussing, N.V., 1912. Geology of the country around Julianehåb, Greenland. Meddelelser om Grønland 38, 1-376.

Villa, I. M., Hermann, J., Müntener, O.,Trommsdorff, V., 2000. 39Ar−40Ar dating of multiply zoned amphibole generations (Malenco, Italian Alps). Contributions to Mineralogy and Petrology 140, 363-381.

Villa, I.M. and Hanchar, J.M., 2013. K-feldspar hygrochronology. Geochimica et Cosmochimica Acta 101, 24-33.

Villa, I.M., De Bièvre, P., Holden, N., Renne, P., 2015a. IUPAC-IUGS recommendation on the half-life of ^{87}Rb. Geochimica et Cosmochimica Acta, 164, 382-385

Waight, T., Baker, J., Willigers, B., 2002. Rb isotope dilution analyses by MC-ICPMS using Zr to correct for mass fractionation: towards improved Rb-Sr geochronology? Chemical Geology 186, 99-116.

Wu, F.Y., Yang, Y.H., Marks, M.A.W., Liu, Z.C., Zhou, Q., Ge, W.C., Yang, J.S., Zhao, Z.F., Mitchell, R.H., Markl, G., 2010. In situ U-Pb, Sr, Nd and Hf isotopic analysis of eudialyte by LA-(MC)-ICP-MS. Chemical Geology 273, 8-34.

Fig. 1 Geological map of the Ilímaussaq complex from Upton (2013), after Ferguson (1964), Andersen *et al.* (1988) and Sørensen (2001). Red arrow marks sampling location of kakortokite Unit 0.

Fig. 2(a) Outcrop of Unit 0 (see Fig. 1) with thin section photographs **(b,c,d)** in cross-polarized (xpl) and plane-polarized light (ppl). **(b)** White kakortokite enriched in alkali feldspar laths, nepheline (white-grey in ppl and xpl) and minor eudialyte (pinkish in ppl, low birefringence). Arfvedsonite (black-green), fluorite and aegirine (green) occur interstitially. **(c)** Saccharoidal fine grained red kakortokite, comprising euhedral eudialyte and nepheline, larger crystals of sodalite (white in ppl, isotropic), alkali feldspar laths and interstitial arfvedsonite and aegirine. **(d)** Black kakortokite composed of sub- to euhedral arfvedsonite, minor aegirine, euhedral nepheline and eudialyte. Thin sections rotated c. 90˚ relative to their original position.

Fig. 3 BSE images **(a)** White kakortokite comprising alkali feldspar (Kfs + Ab), partially altered eudialyte (Eud + Alt) and interstitial arfvedsonite (Arf), nepheline (Nph) and analcime (Anl). Note turbidity in the albitic zones and holes in the thin section. **(b)** Euhedral nepheline, alkali feldspar and interstitial arfvedsonite enclosing sub-rounded grains of fluor-apatite (Ap) and fluorite (Fl). **(c)** Sub-rounded fluorite and apatite inclusions in arfvedsonite. Arfvedsonite is overgrown by primary aegirine (Aeg-I) and partially replaced by secondary aegirine (Aeg-II). Analcime replaces alkali feldspar and nepheline. **(d)** Black kakortokite with subhedral arfvedsonite, fully replaced pseudomorph after eudialyte, patchy alkali feldspar and analcime. **(e)** Black kakortokite with nepheline, sodalite, analcime, eudialyte and clusters of albite laths enclosed in arfvedsonite. **(f)** Red kakortokite with euhedral Eud, alkali feldspar and sodalite crystals enclosed in arfvedsonite. Sodalite and nepheline are partially replaced by analcime (Anl) and arfvedsonite by aegirine-II.

Fig. 4(a) Pb-Pb isochron diagram, defining an isochron of 1159 ± 17 Ma (n=12). **(b)** ^{238}U-^{206}Pb isochron plot illustrating minor disturbance of U-Pb systematics in some minerals. An age of 1173 ± 16 Ma (n=8) was calculated by omitting the labelled outliers. **(c)** ^{235}U-^{207}Pb isochron plot showing similar anomalies as above and defining an isochron age of 1168.5 ± 8.8 Ma (n=8). Ages are calculated using errors of 0.3% for $^{206}Pb/^{204}Pb$, 0.1% for $^{207}Pb/^{204}Pb$ and 0.2% for both U/Pb ratios based on external reproducibility of standards. In run analytical errors (2σ) are smaller than symbols used.

Fig. 5 Sm-Nd isochron diagram for TIMS and MC-IPMS data. A regression that excludes outliers (535)021-arf, 019-fsp and 020-wr yields 1156 ± 53 Ma (MSWD = 0.23, n = 11), using errors of 0.02% $^{147}Sm/^{144}Nd$ and 0.003% for $^{143}Nd/^{144}Nd$ based on external reproducibility of standards. In run analytical errors are typically smaller than symbol size used.

Fig. 6a) Rb-Sr isochron diagram. Note the high Rb/Sr of the alkali feldspars relative to whole rock, amphibole and eudialyte (Detail of circled data in (b). A regression through all points yields an errorchron with high MSWD and a falsely young age of 1091 ± 6.3 Ma (black line). A three-point feldspar regression yields 1106 ± 94 Ma (MSWD=25, n=3) with a poorly defined $^{87}Sr/^{86}Sr_i$ of 0.5 ± 1.4. Grey line represents 1160 Ma trend for reference. **(b)** A regression that excludes all feldspars, as well as 535021-arf, yields an errorchron age of 1237 ± 21 Ma with $^{87}Sr/^{86}Sr_i$ = 0.707 and high MSWD. Ages are calculated using errors of 0.003% for $^{87}Sr/^{86}Sr$ and 0.2% for $^{87}Rb/^{86}Sr$ based on external reproducibility of standards. In run analytical errors are smaller than symbol size used.

Fig. 7 $^{40}Ar/^{39}Ar$ age spectra from single crystal step-heating experiments on arfvedsonite from the black kakortokite (531019-0B). **(a-d)** Gas release patterns for four grains, showing

the calculated age (Ma) per heating step in the lower panel, the % of radiogenic $^{40}Ar^*$ in the middle panel, and the Ca/K ratio in the upper panel, plotted against the cumulative % of ^{39}Ar.

Fig. 8 Comparison to published Sm-Nd data from other Ilímaussaq whole rocks (WR) and mineral separates (Min). Grey line and shading mark the 1160 Ma reference isochron with $^{143}Nd/^{144}Nd_i = 0.51110 \pm 4$.

Fig. 9 Compilation of published Rb-Sr data for Ilímaussaq. Polylithionite samples from Moorbath *et al.* (1960) plot just below the 1091 Ma alkali feldspar trend (from Fig. 6a), also suggesting loss of ^{87}Sr. Individual polylithionite Rb-Sr dates and reported isochron ages from Waight *et al.* (2002) and Blaxland *et al.* (1967b) are recalculated using ^{87}Rb $\lambda = 1.397*10^{-11}$ a^{-1}. Inset shows details for low Rb/Sr samples (e.g. eudialyte, amphibole and whole rocks). The 1160 Ma trend (grey line) is shown for reference.

Fig. 10 Whole rock Sr **(a)** and Rb **(b)** contents across the layered kakortokite sequence (circles: XRF data from Bailey *et al.* (2001); stars: whole rock ID-data, this study). Note sharp increase in Sr contents between unit 0 and 3. Whole rock Sr budgets are controlled by eudialyte, with the highest Sr contents in red kakortokites. Outlier unit 3 black contains secondary Sr-rich eudialyte associated with gittinsite (Borst *et al.*, 2016). Rb budgets are controlled by alkali feldspar with maxima in white kakortokites.

Fig. 11 Compilation of U-Pb, Sm-Nd, Rb-Sr and Ar-Ar ages for Ilímaussaq. See Table 1 for details and references.

Fig. 12 ε_{Ndi} vs $^{87}Sr/^{86}Sr_i$ evolution diagram. Red shaded area shows the wide range in $^{87}Sr/^{86}Sr_i$ and narrow range in ε_{Ndi} for most Ilímaussaq rocks. Maximum range of Ilímaussaq ε_{Ndi} values from data of Paslick (1993), Stevenson *et al.* (1997), Marks *et al.* (2004) and Wu *et al.* (2010), with the widest range recorded in the augite syenite (+0.4 and -5.7). Other

Gardar data shown for comparison, from Andersen (1997), Bartels *et al.* (2015), Blaxland *et al.* (1976a,b; 1978), Goodenough *et al.* (2002), Halama *et al.* (2003, 2004, 2005), Marks *et al.* (2004), Paslick *et al.* (1993), Pearce and Leng (1996) and Taubald *et al.* (2004). Bulk Silicate Earth (BSE) is calculated assuming present-day $^{87}Rb/^{86}Sr$ of 0.0827 and $^{87}Sr/^{86}Sr$ of 0.7045 (DePaolo, 1988). Depleted MORB mantle (DMM) values are from DePaolo (1981) and Goldstein (1984). Initial ratios for Ilímaussaq and mantle and crustal reservoirs are calculated for t = 1160 Ma. Other Gardar data are shown for t = emplacement (see ages in text). Inset shows evolution curves related to (1) preferential uptake of ^{87}Sr from Ketilidian crust (Blaxland *et al.*, 1976a,b), (2) assimilation-fractional crystallization (AFC) of a basaltic-syenitic-agpaitic melt assimilating Ketilidian crust (Stevenson *et al.*, 1997) and (3) mixing trends between more primitive Gardar magmas (lower Nd, higher Sr) and (3a) Ketilidian upper crust or (3b) Archaean lower crust (Andersen, 1997; Halama *et al.*, 2003; 2004; Marks *et al.*, 2004).

TABLE 1. COMPILATION OF U-PB, SM-ND, RB-SR AND AR-AR AGE DATA FOR THE ILÍMAUSSAQ COMPLEX. REPORTED AGES ARE LISTED ALONG WITH THE CONSTANTS USED IN THE ORIGINAL WORK, AND RECALCULATED USING THE MODERN DECAY CONSTANTS.

U-Pb data

Age (Ma)	MSWD	Reference	Type	Rock type	Phases [a]	λ_{238U}	λ_{235U}	Fig. 11
1160 ± 5	0.55	Krumrei et al. (2006)	Discordia age	Augite syenite	Baddeleyite	$1.55*10^{-10}$	$9.85*10^{-10}$	1
1166 ± 9	-	Heaman and Upton, cited in Upton et	Unspecified	Alkali granite	Zircon			2

			al. (2003)							
1018-1134 ± 29-34		-	Wu et al. (2010)	Discordia ages	Agpaites	Eud				3
1159 ± 17		0.96	This study	Pb-Pb isochron	Kakortokites	WR, Amph, Eud, Afsp				4a
1173 ± 16		11.3	´´	^{235}U-^{207}Pb isochron	Kakortokites	WR, Amph, Eud, Afsp				4b
1168.5 ± 8.8		0.82	´´	^{238}U-^{206}Pb isochron	Kakortokites	WR, Amph, Eud, Afsp				4c

Sm-Nd data

Age (Ma)	**Recalculated**	**MSWD**	**Reference**	**Type**	**Rock type**	**Phases**	**$\lambda_{^{144}Sm}$[b]**		**$^{143}Nd/^{144}Nd_i$**	**Fig. 11**
1130 ± 50		0.08	Paslick et al. (1993)	WR-Min isochron	Augite syenite	Px, Afsp, Mgt	$6.54*10^{-12}$	(2)	0.51112 ± 4	5
1160 ± 30		3.7	Marks et al. (2004)	WR-Min isochron	All units	WR, Aeg, Aug, Amph			-	6a
	1131 ± 130	2.9	,,						0.51111 ± 9	6b
1128 ± 63		3.6	Wu et al. (2010)	Mineral isochron	Agpaites	Eud			-	7
1156 ± 53		0.23	This study	WR-Min isochron	Kakortokites	WR, Amph, Eud, Afsp			0.51110 ± 4	8

Rb-Sr data

Age (Ma)	**Recalculated**	**MSWD**	**Reference**	**Type**	**Rock type**	**Phases**	**$\lambda_{^{87}Rb}$[b]**		**$^{87}Sr/^{86}Sr_i$**	**Fig. 11**
1188 ± 30		5.63	Blaxland et al. (1976b)	WR isochron	All units	Whole rock	$1.39*10^{-11}$	(3)	0.706 ± 2	
1150 ±		3.3	´´	WR	Kakorto	Whole	´´		0.711	

50		2		isochron	kites	rock			± 2	
1168 ± 21		3.65	´´	WR isochron	Agpaites	Whole rock	´´		0.710 ± 2	
	1162 ± 21	53	´´				1.397*10^{-11}	(4)		9
1161.2 ± 2.3			Waight et al. (2002)	Model isochron	Kakortokite	Afsp	1.42*10^{-11}	(1)	0.70500 ± 2	
1160.1 ± 2.3			´´	2-Min isochron	Kakortokite	Eud, Afsp	´´		0.71149 ± 2	
	1179.2 ± 2.3	-	´´				1.397*10^{-11}	(4)		10
1086 ± 24			Moorbath et al. (1960)	Mineral isochron	Agpaitic pegmatite	Polylithionite	1.39*10^{-11}	(3)	-	
	1081 ± 24		´´				1.397*10^{-11}	(4)		11
1091 ± 6.3		10737	This study	WR-Min isochron	Kakortokite	WR, Amph, Eud, Afsp	´´		0.70 ± 4	
1106 ± 94		25	´´	WR-Min isochron	,,	Afsp	´´		0.5 ± 1.4	12a
1237 ± 21		9811	´´	WR-Min isochron	,,	WR, Amph, Eud	´´		0.707 ± 3	12b

Ar-Ar data

Age (Ma)[c]	**Recalculated**	**MSWD**	**Reference**	**Type**	**Rock type**	**Phases**	**$\lambda_{^{40}K}$ [b]**		**FCT age (Ma)[b]**	**Fig. 11**
1143-1152 ± 3.6-4.4		2 - 5.4	Krumrei et al. (2006)	Plateau ages	All Units	Amph	5.543*10^{-10}	(1)	28.02 (6)	13a
	1150.5-1161.2	-					5.8*10^{-10}	(5)	28.172 (7)	13b
1156.5 ± 1.4 (7.7)		1.4	This study	Plateau age	Kakortokites	Amph	´´		´´	14
1156.8 ± 1.4 (5.7)			´´						28.294 ± 0.036 (8)	

	´´	28.30
1157.1 ± 1.4 (5.7)		5 ± 0.036 (9)
	´´	28.20
1157.5 ± 1.4 (7.7)		1 ± 0.012 (10)

a Abbreviations: Aeg = aegirine, Afsp = alkali feldspar, Amph = amphibole, Aug= augite, Eud = eudialyte, FCT = Fish Canyon Tuff, Mgt = magnetite, Px = pyroxene, WR = whole rock.

b References for decay constants (λ in a^{-1}) and FCT ages: (1) Steiger and Jäger, 1977; (2) Lugmair and Marti, 1978; (3) Aldrich et al., 1956; (4) Villa et al., 2015a; (5) Min et al., 2000; (6) Renne et al., 1998; (7) Rivera et al., 2011; (8) Renne et al., 2011; (9) Renne et al., 2010; (10) Kuiper et al., 2008).

c Errors in brackets represent external errors related to uncertainty on the decay constant and FCT age

Highlights

- Ilímaussaq whole rock-mineral U-Pb, Sm-Nd and Rb-Sr isochron data are compared
- Amphibole $^{40}Ar/^{39}Ar$ dating gives agpaitic crystallization age of 1156.6 ± 1.4 Ma
- U-Pb isochrons provide reasonable age constraints for zircon-free agpaitic rocks
- Sm-Nd isotope system is unaffected by late-magmatic hydrothermal alteration
- Disturbed Rb-Sr system demonstrates mobility of LILE in agpaitic systems

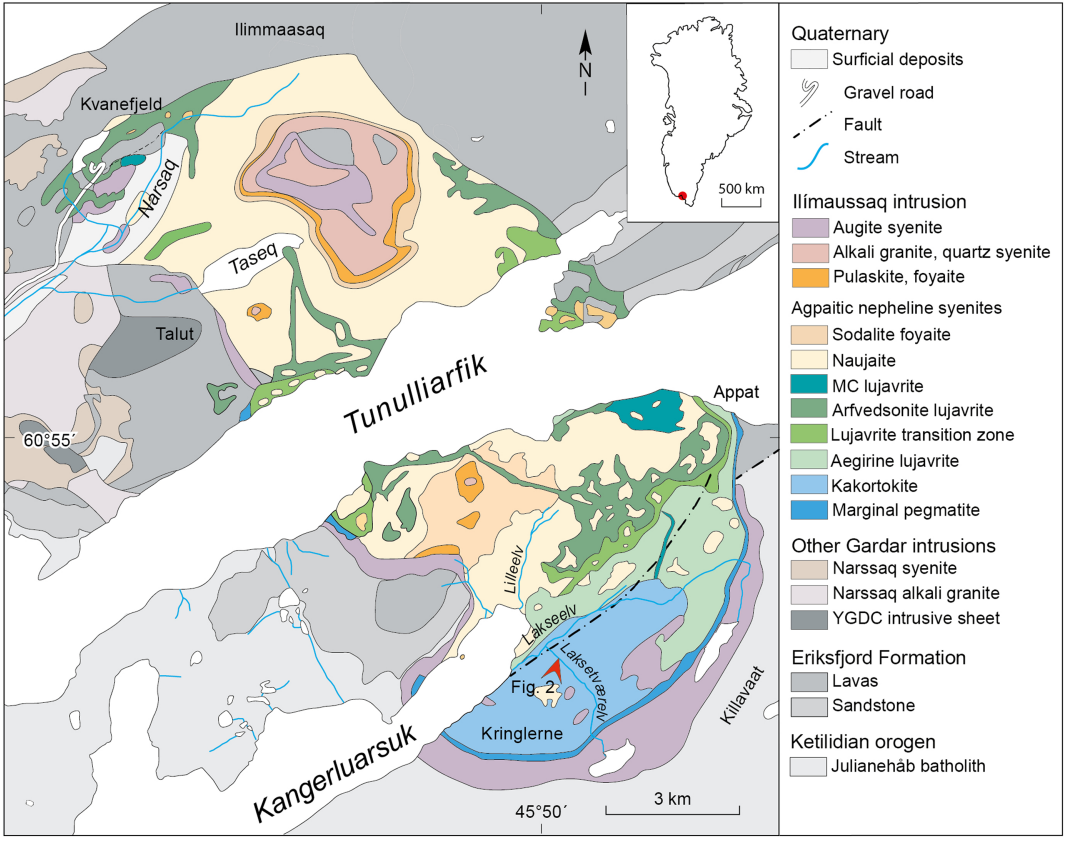
Ilimmaasaq
Kvanefjeld
Narsaq
Taseq
Talut
Tunulliarfik
Appat
60°55´
Lilleelv
Lakseelv
Lakselvværelv
Fig. 2
Kringlerne
Killavaat
Kangerluarsuk
45°50´
3 km
N
500 km
Quaternary
Surficial deposits
Gravel road
Fault
Stream
Ilímaussaq intrusion
Augite syenite
Alkali granite, quartz syenite
Pulaskite, foyaite
Agpaitic nepheline syenites
Sodalite foyaite
Naujaite
MC lujavrite
Arfvedsonite lujavrite
Lujavrite transition zone
Aegirine lujavrite
Kakortokite
Marginal pegmatite
Other Gardar intrusions
Narssaq syenite
Narssaq alkali granite
YGDC intrusive sheet
Eriksfjord Formation
Lavas
Sandstone
Ketilidian orogen
Julianehåb batholith

Figure 1

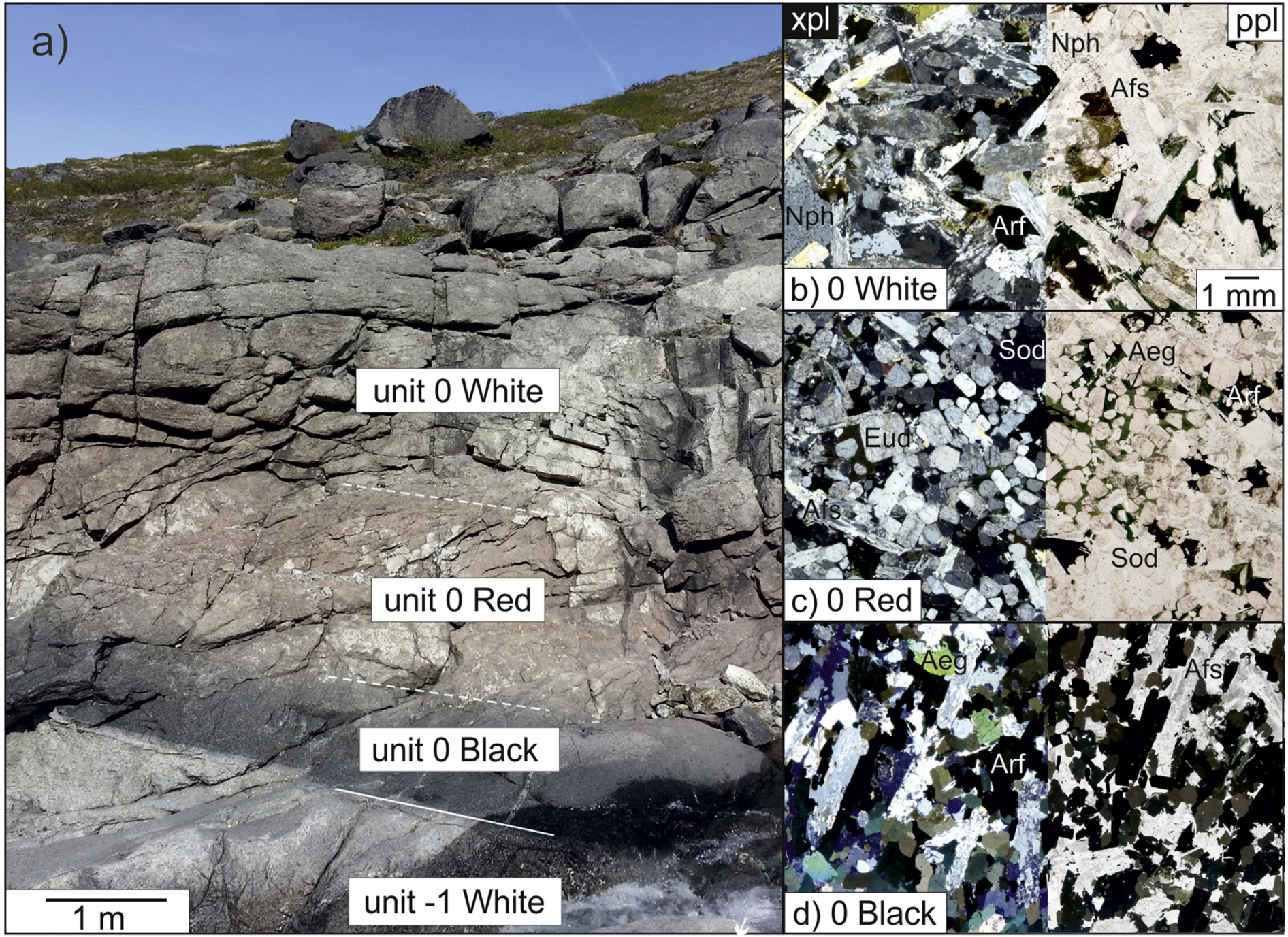
a)
unit 0 White
unit 0 Red
unit 0 Black
unit -1 White
1 m
xpl
Nph
Arf
b) 0 White
ppl
Nph
Afs
1 mm
Sod
Eud
Afs
c) 0 Red
Aeg
Arf
Sod
Aeg
Arf
d) 0 Black
Afs

Figure 2

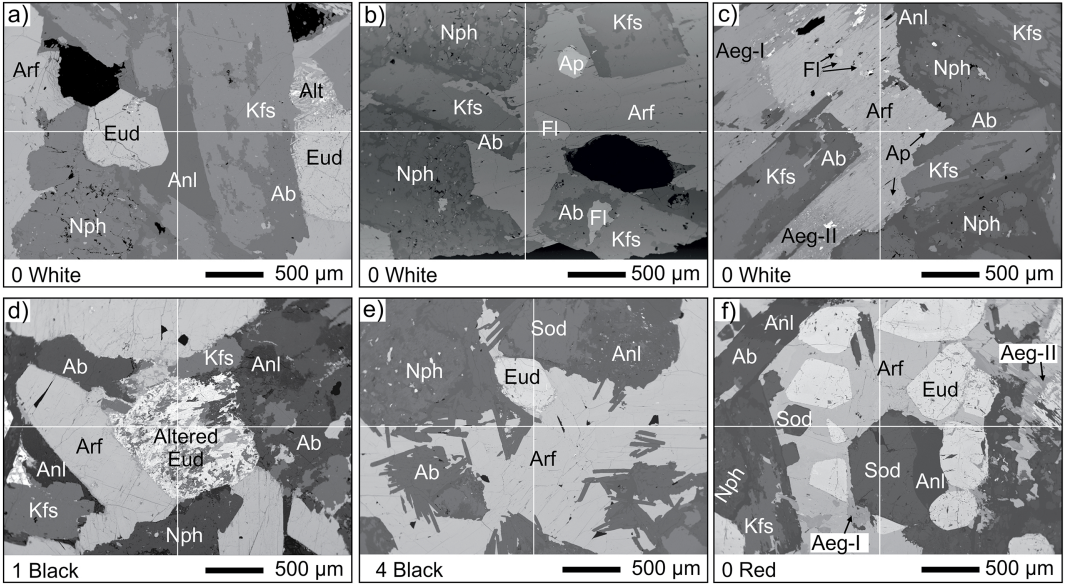
a)
Arf
Alt
Kfs
Eud
Eud
Anl
Ab
Nph
0 White
500 µm
b)
Nph
Kfs
Ap
Kfs
Arf
Fl
Ab
Nph
Ab
Fl
Kfs
0 White
500 µm
c)
Anl
Kfs
Aeg-I
Fl
Nph
Arf
Ab
Ab
Ap
Kfs
Kfs
Nph
Aeg-II
0 White
500 µm
d)
Ab
Kfs
Anl
Arf
Altered
Eud
Ab
Anl
Kfs
Nph
1 Black
500 µm
e)
Sod
Anl
Nph
Eud
Ab
Arf
4 Black
500 µm
f)
Anl
Ab
Aeg-II
Arf
Eud
Sod
Nph
Sod
Anl
Kfs
Aeg-I
0 Red
500 µm

Figure 3

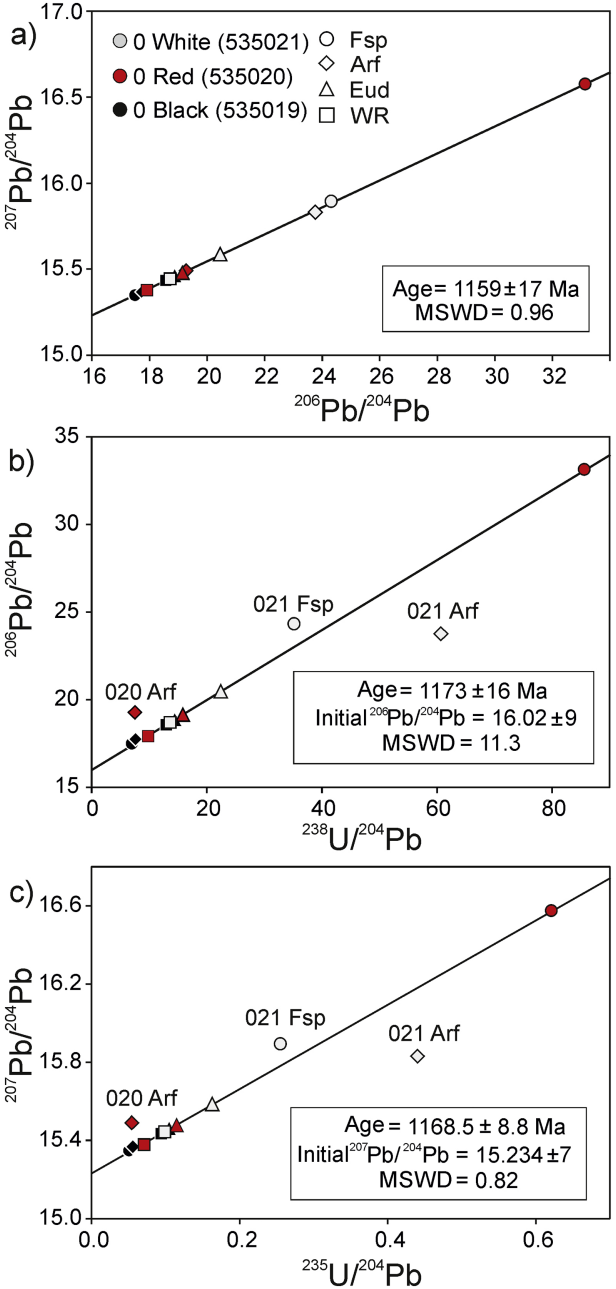
a)
0 White (535021)
0 Red (535020)
0 Black (535019)
Fsp
Arf
Eud
WR
Age= 1159±17 Ma
MSWD= 0.96
$^{207}Pb/^{204}Pb$
$^{206}Pb/^{204}Pb$
b)
021 Fsp
021 Arf
020 Arf
Age= 1173 ±16 Ma
Initial $^{206}Pb/^{204}Pb$ = 16.02 ±9
MSWD = 11.3
$^{206}Pb/^{204}Pb$
$^{238}U/^{204}Pb$
c)
021 Fsp
021 Arf
020 Arf
Age= 1168.5 ± 8.8 Ma
Initial $^{207}Pb/^{204}Pb$ = 15.234 ±7
MSWD= 0.82
$^{207}Pb/^{204}Pb$
$^{235}U/^{204}Pb$

Figure 4

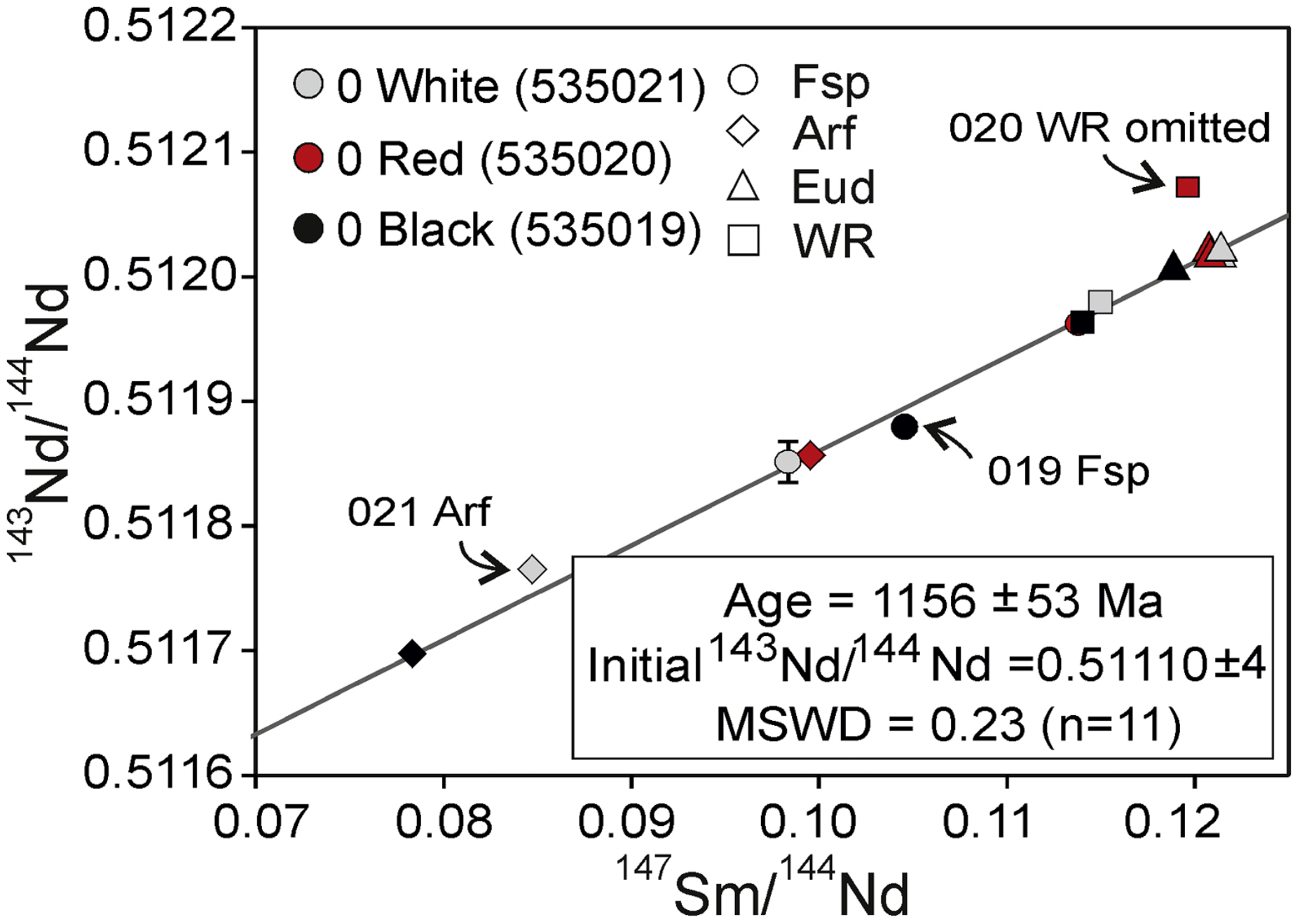
0.5122
0.5121
0.5120
0.5119
0.5118
0.5117
0.5116
0.07
0.08
0.09
0.10
0.11
0.12
$^{143}Nd/^{144}Nd$
$^{147}Sm/^{144}Nd$
0 White (535021)
0 Red (535020)
0 Black (535019)
Fsp
Arf
Eud
WR
020 WR omitted
019 Fsp
021 Arf
Age = 1156 ± 53 Ma
Initial $^{143}Nd/^{144}Nd$ = 0.51110 ± 4
MSWD = 0.23 (n=11)

Figure 5

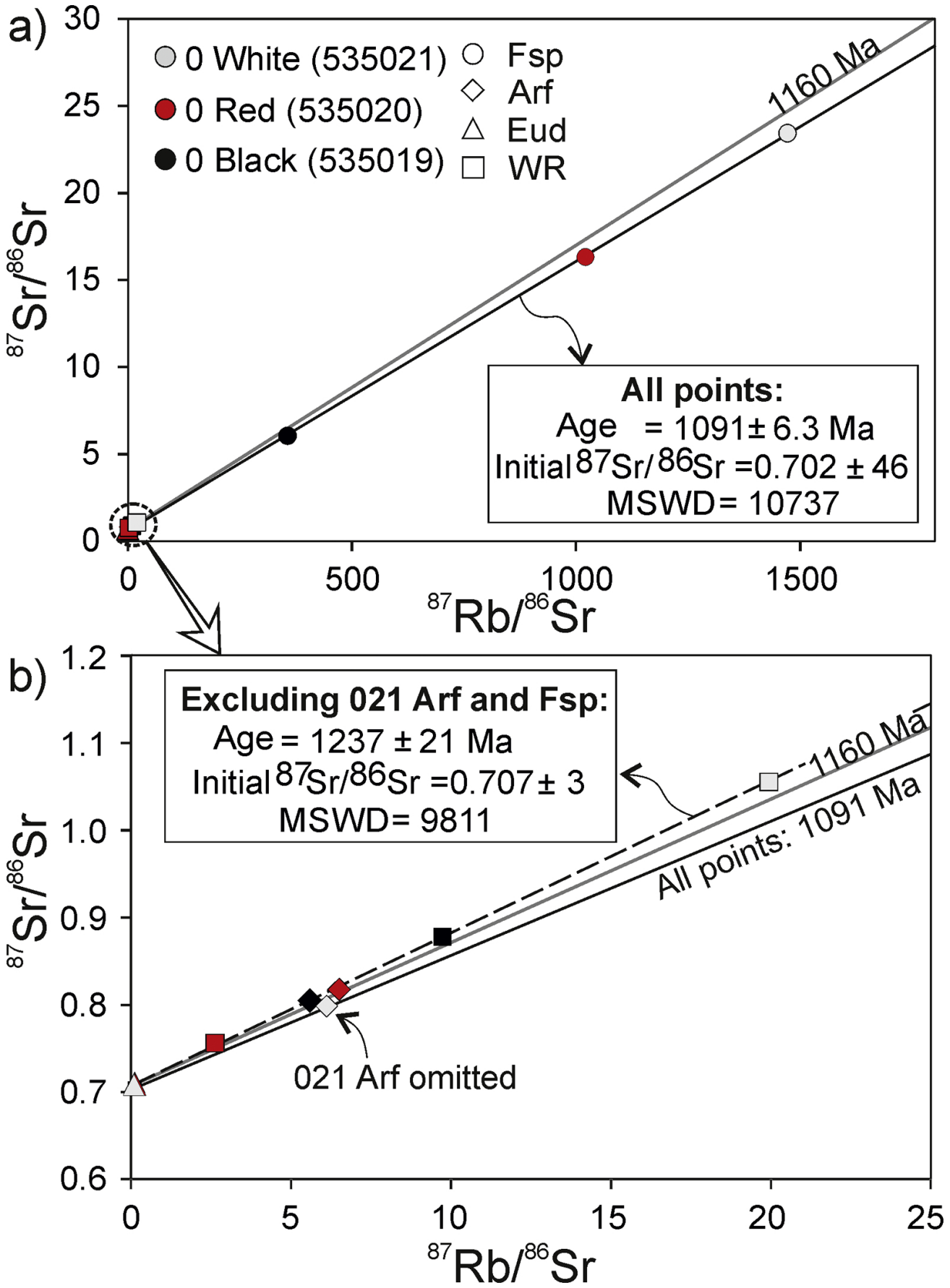
a)
0 White (535021)
0 Red (535020)
0 Black (535019)
Fsp
Arf
Eud
WR
1160 Ma
All points:
Age = 1091± 6.3 Ma
Initial 87Sr/86Sr =0.702 ± 46
MSWD= 10737
87Sr/86Sr
87Rb/86Sr
b)
Excluding 021 Arf and Fsp:
Age = 1237 ± 21 Ma
Initial 87Sr/86Sr =0.707± 3
MSWD= 9811
1160 Ma
All points: 1091 Ma
021 Arf omitted
87Sr/86Sr
87Rb/86Sr

Figure 6

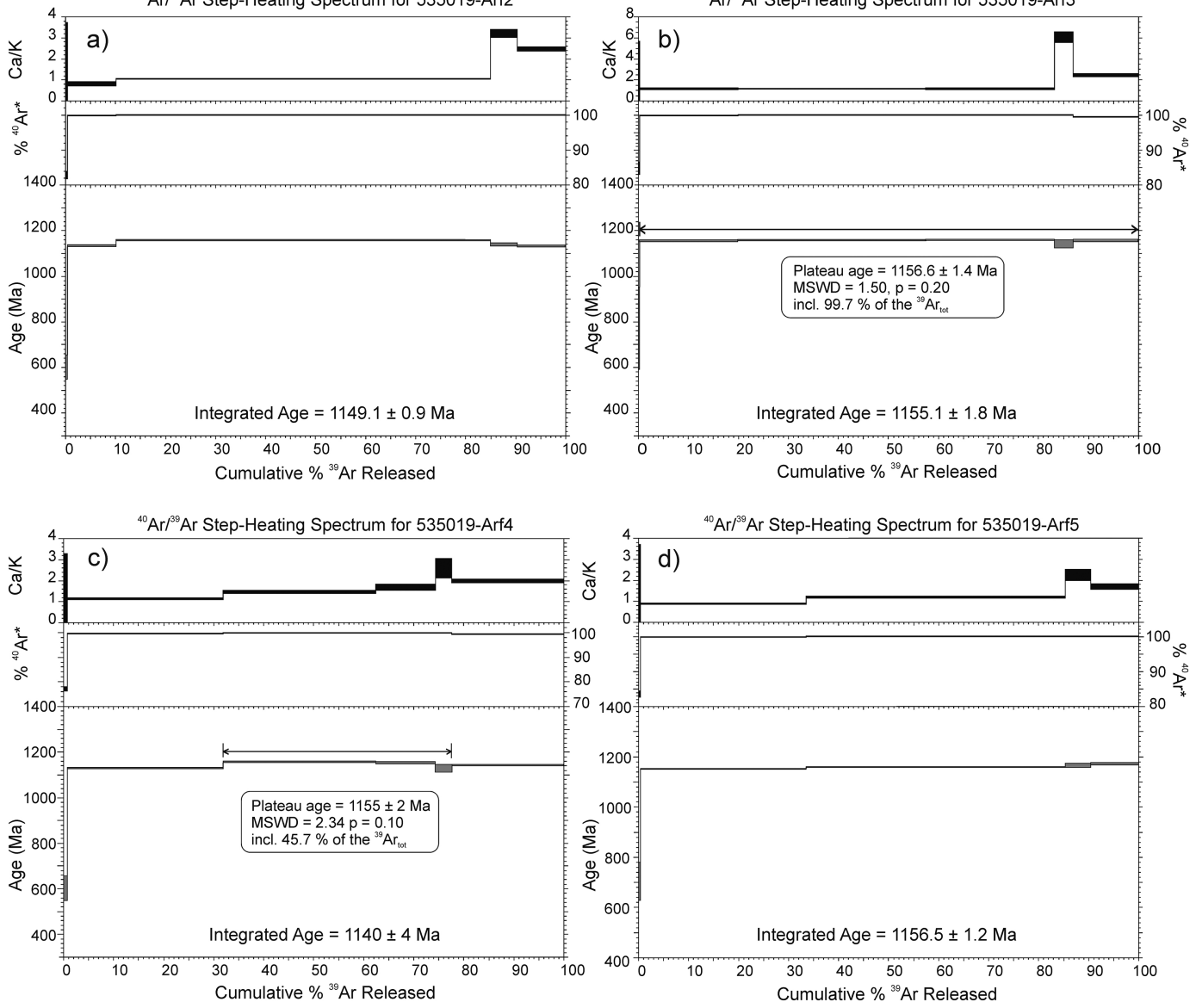
40Ar/39Ar Step-Heating Spectrum for 535019-Arf2
a)
Ca/K
% 40Ar*
Age (Ma)
Integrated Age = 1149.1 ± 0.9 Ma
Cumulative % 39Ar Released
40Ar/39Ar Step-Heating Spectrum for 535019-Arf3
b)
Plateau age = 1156.6 ± 1.4 Ma
MSWD = 1.50, p = 0.20
incl. 99.7 % of the 39Artot
Integrated Age = 1155.1 ± 1.8 Ma
40Ar/39Ar Step-Heating Spectrum for 535019-Arf4
c)
Plateau age = 1155 ± 2 Ma
MSWD = 2.34 p = 0.10
incl. 45.7 % of the 39Artot
Integrated Age = 1140 ± 4 Ma
40Ar/39Ar Step-Heating Spectrum for 535019-Arf5
d)
Integrated Age = 1156.5 ± 1.2 Ma

Figure 7

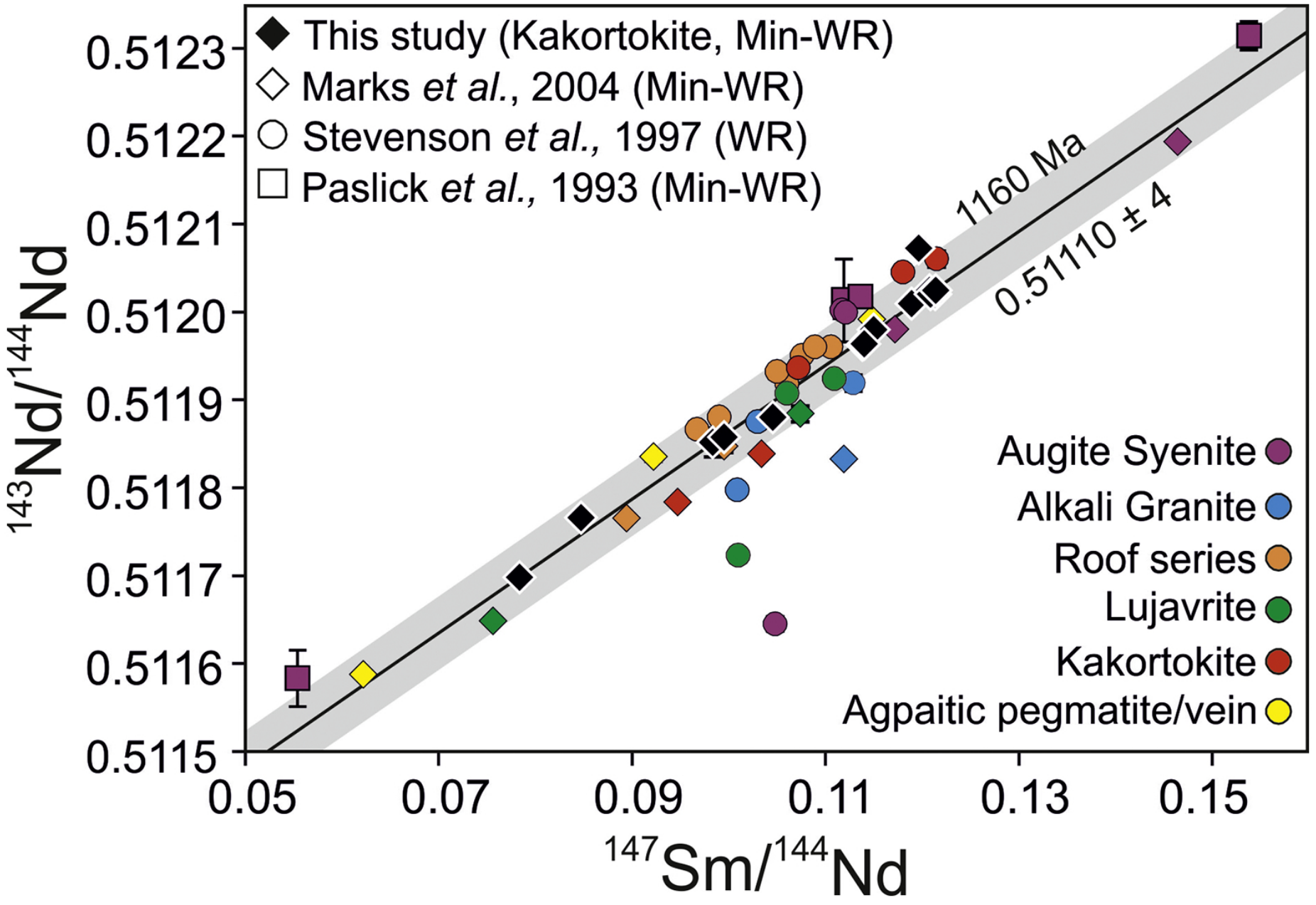
This study (Kakortokite, Min-WR)
Marks et al., 2004 (Min-WR)
Stevenson et al., 1997 (WR)
Paslick et al., 1993 (Min-WR)
1160 Ma
0.51110 ± 4
Augite Syenite
Alkali Granite
Roof series
Lujavrite
Kakortokite
Agpaitic pegmatite/vein
0.5123
0.5122
0.5121
0.5120
0.5119
0.5118
0.5117
0.5116
0.5115
0.05
0.07
0.09
0.11
0.13
0.15
143Nd/144Nd
147Sm/144Nd

Figure 8

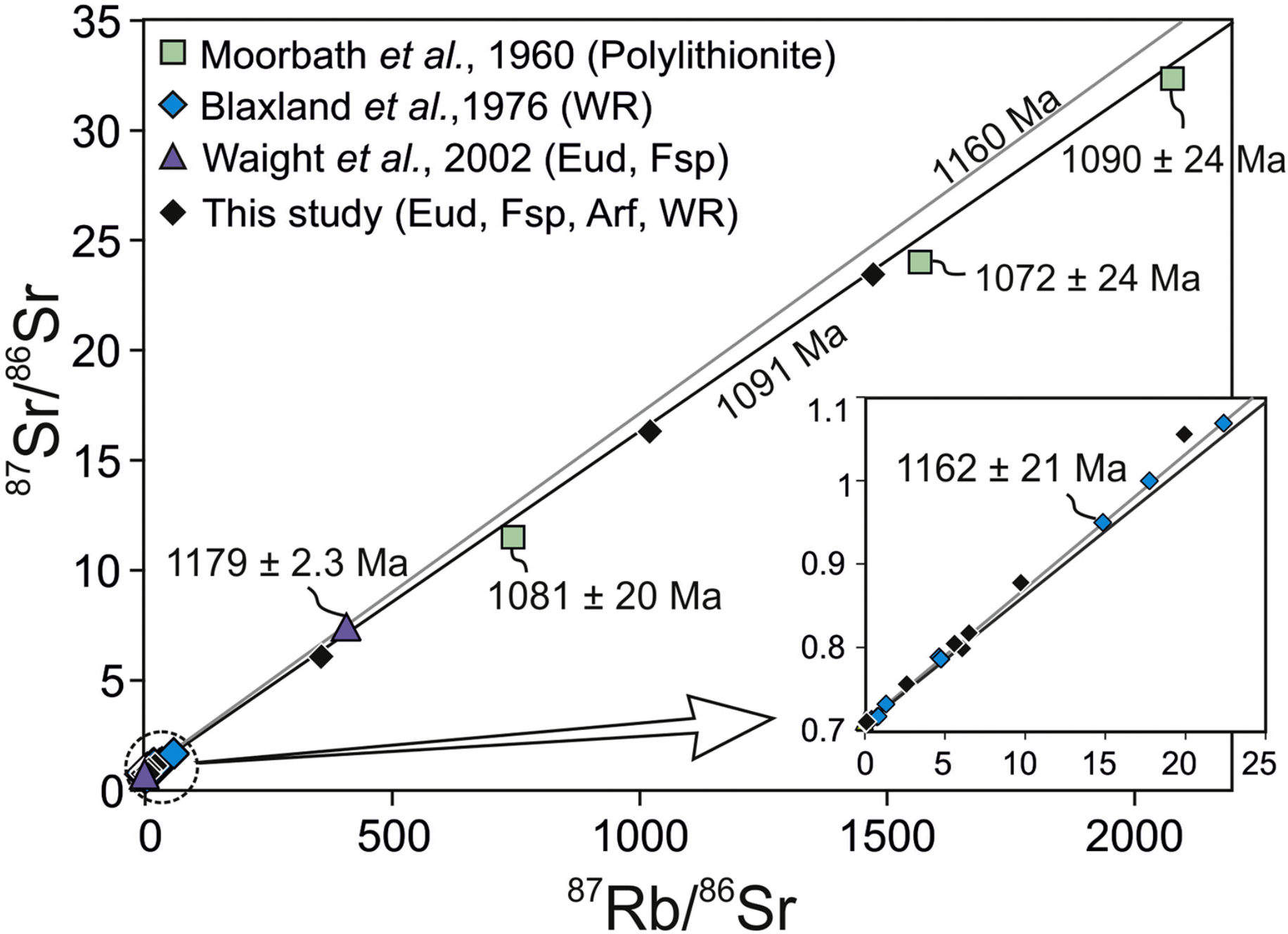
Moorbath et al., 1960 (Polylithionite)
Blaxland et al.,1976 (WR)
Waight et al., 2002 (Eud, Fsp)
This study (Eud, Fsp, Arf, WR)
1160 Ma
1090 ± 24 Ma
1072 ± 24 Ma
1091 Ma
1179 ± 2.3 Ma
1081 ± 20 Ma
1162 ± 21 Ma
87Sr/86Sr
87Rb/86Sr
0
5
10
15
20
25
30
35
500
1000
1500
2000
0.7
0.8
0.9
1
1.1

Figure 9

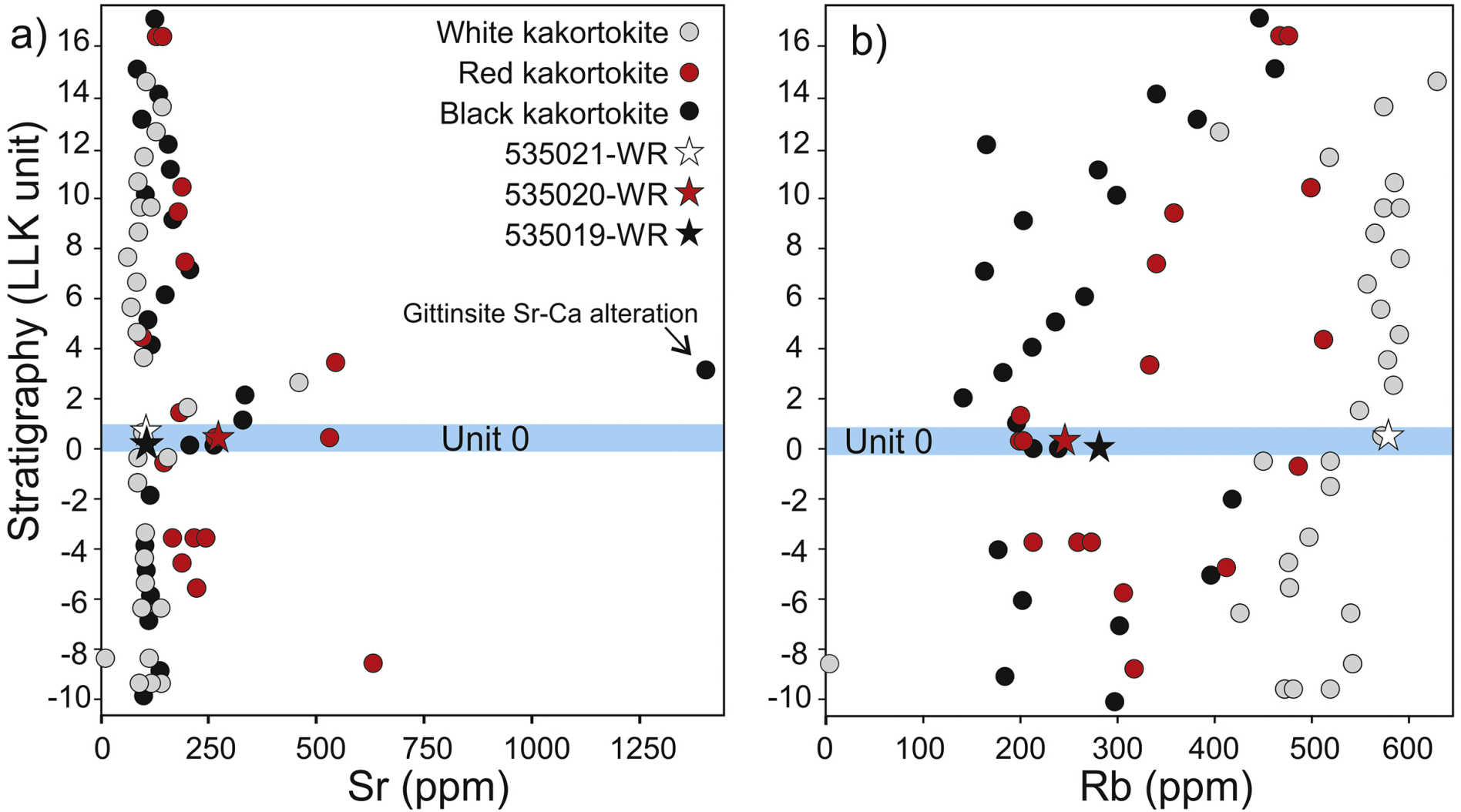
a)
b)
White kakortokite
Red kakortokite
Black kakortokite
535021-WR
535020-WR
535019-WR
Gittinsite Sr-Ca alteration
Unit 0
Unit 0
Stratigraphy (LLK unit)
Sr (ppm)
Rb (ppm)
16
14
12
10
8
6
4
2
0
-2
-4
-6
-8
-10
0
250
500
750
1000
1250
100
200
300
400
500
600

Figure 10

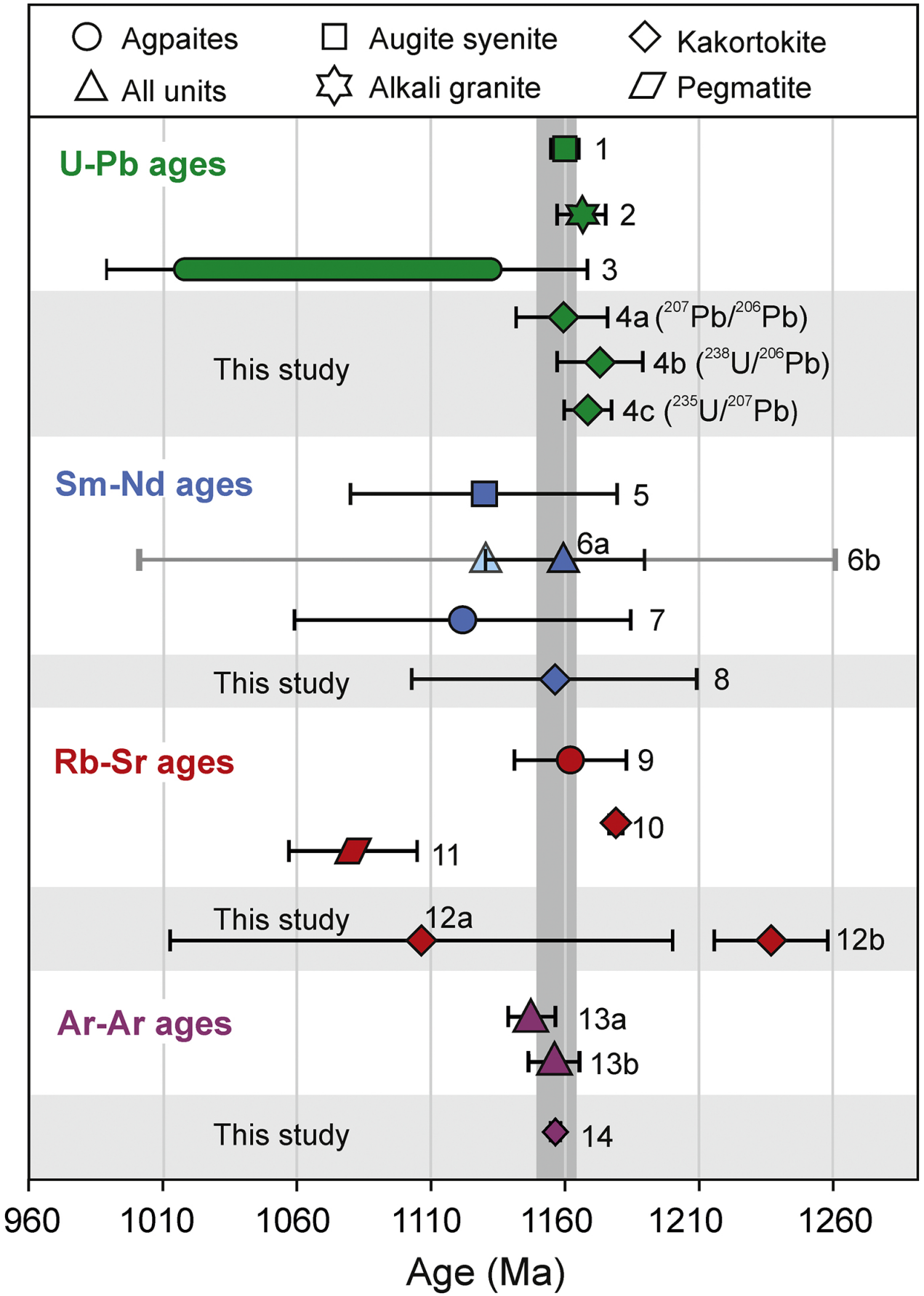
Agpaites
Augite syenite
Kakortokite
All units
Alkali granite
Pegmatite
U-Pb ages
1
2
3
4a (207Pb/206Pb)
This study
4b (238U/206Pb)
4c (235U/207Pb)
Sm-Nd ages
5
6a
6b
7
This study
8
Rb-Sr ages
9
10
11
This study
12a
12b
Ar-Ar ages
13a
13b
This study
14
960
1010
1060
1110
1160
1210
1260
Age (Ma)

Figure 11

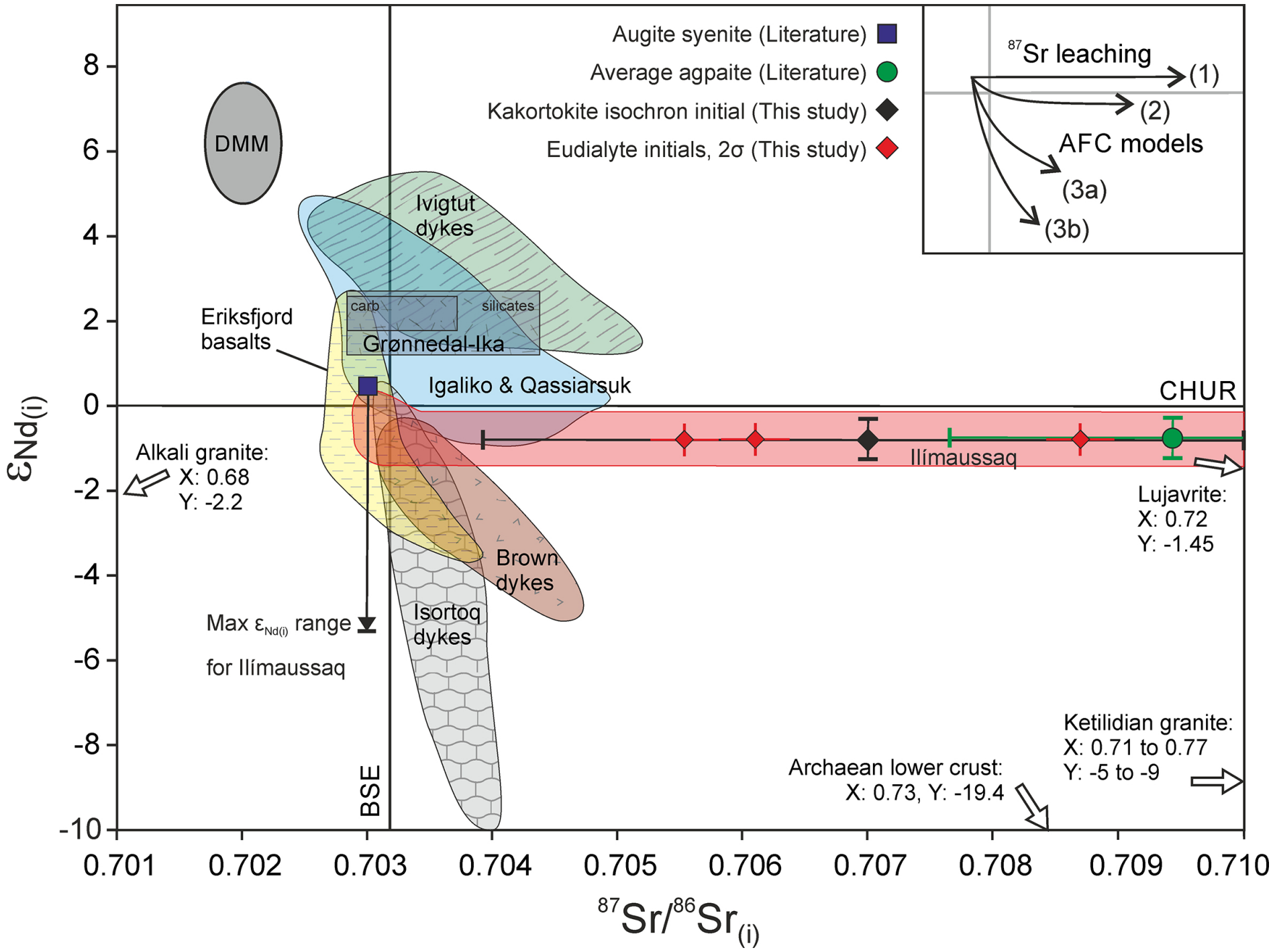
Augite syenite (Literature)
Average agpaite (Literature)
Kakortokite isochron initial (This study)
Eudialyte initials, 2σ (This study)
87Sr leaching
(1)
(2)
AFC models
(3a)
(3b)
DMM
Ivigtut dykes
carb
silicates
Eriksfjord basalts
Grønnedal-Ika
Igaliko & Qassiarsuk
CHUR
Ilímaussaq
Alkali granite:
X: 0.68
Y: -2.2
Lujavrite:
X: 0.72
Y: -1.45
Brown dykes
Isortoq dykes
Max εNd(i) range
for Ilímaussaq
BSE
Archaean lower crust:
X: 0.73, Y: -19.4
Ketilidian granite:
X: 0.71 to 0.77
Y: -5 to -9
εNd(i)
87Sr/86Sr(i)
8
6
4
2
0
-2
-4
-6
-8
-10
0.701
0.702
0.703
0.704
0.705
0.706
0.707
0.708
0.709
0.710

Figure 12